February 2016
Master's Dissertation

Study on the power and polarization dependence of ultra-narrow electromagnetically induced absorption spectra of ^{85}Rb atoms in degenerate two-level system

Graduate School of Chosun University

Department of Photonic Engineering

Muhammad Mohsin Qureshi

Study on the power and polarization dependence of ultra-narrow electromagnetically induced absorption spectra of ^{85}Rb atoms in degenerate two-level system

축퇴된 이준위 루비듐 원자의 매우 좁은 선폭을
가지는 EIA 스펙트라의 파워 및 편광 의존성 연구

February 25, 2016

Graduate School of Chosun University

Department of Photonic Engineering

Muhammad Mohsin Qureshi

Study on the power and polarization dependence of ultra-narrow electromagnetically induced absorption spectra of ^{85}Rb atoms in degenerate two-level system

Advisor: Prof. Jin-Tae Kim

This dissertation is submitted to the Graduate School of Chosun University in partial fulfillment of the requirements for the degree of Masters in Science

October 2015

Graduate School of Chosun University

Department of Photonic Engineering

Muhammad Mohsin Qureshi

This is to certify that the Master's thesis of **Muhammad Mohsin Qureshi** has successfully met the dissertation requirements of Chosun University

Chairman (Chosun Univ.): Prof. Hyun Su Kim……

Member (Chosun Univ.): Prof. Jin-Tae Kim……

Member (Chonnam Univ.): Prof. Heung-Ryoul Noh……. …

November 2015

Graduate School of Chosun University

Table of Contents

Figure Captions

List of Tables

초록

축퇴된 이준위 루비듐 원자의 매우 좁은 선폭을 가지는 EIA 스펙트라의 파워 및 편광 의존성 연구

Muhammad Mohsin Qureshi

Advisor: Prof. Jin-Tae Kim, Ph.D.

Graduate School of Chosun University

Department of Photonic Engineering

^{85}Rb D_2 $F_g = 3 \rightarrow F_e = 4$ 천이선의 축퇴된 이준위 시스템에서 펌프 빔의 편광과 파워 변화에 따른 매우 좁은 선폭을 가지는 EIA 신호 형상들에 관한 연구를 수행하였다. 두 다른 실험에서 프로브 빔의 편광은 우원 편광과 수평 선 편광으로 각 각 고정하고, 펌프 빔은 프로브 빔의 편광에서 시작하여 프로브 빔에 수직한 편광으로 점점 변화시켰다. 그러므로 원형 편광의 경우 우원 편광에서 점점 선형 편광을 지나 좌원 편광으로 변화하고 선편광의 경우는 수직 편광에서 편광을 변화시켜 수평 편광으로 변화 시켰다. 두 대의 독립적인 펌프 및 프로브 레이저를 사용하는 경우에 넓은 레이저 선폭에 의한 좁은

선폭의 EIA 신호를 관측하지 못하기 때문에 실험실에서 제작한 하나의 레이저와 AOM 들을 이용하여 펌프 빔과 프로브 빔을 준비하였다. 이론적으로 좁은 선폭을 가지는 EIA 신호는 펌프 빔에 의해 준비된 축퇴된 이준위 시스템의 광학 블로호 방정식으로부터 프로브 빔의 흡수 계수를 계산 함으로서 얻어졌다. 원형 편광의 경우 EIA 신호가 같은 편광을 가지는 경우에도 이론에서 얻은 바와 같이 EIA 신호가 얻어졌으며, EIA 신호는 펌프 빔의 파워가 증가하는 경우 EIA 신호가 줄어드는 것을 관측할 수가 있었다. 이 경우 펌프 빔의 편광이 선형 편광인 경우가 제일 강한 신호를 줌을 이론으로 얻을 수 있었으며, 실험에서도 또한 같은 결과를 얻을 수가 있었다. 전반적인 펌프 빔의 편광에 따른 관측된 EIA 신호들은 계산된 결과와 유사한 경향을 보이는 것을 알 수가 있었다.

Abstract

Study on power and polarization dependences of ultra-narrow electromagnetically induced absorption (EIA) spectra of ^{85}Rb atoms in degenerate two-level system

Muhammad Mohsin Qureshi
Advisor: Prof. Jin-Tae Kim, Ph.D.
Department of Photonic Engineering
Graduate School of Chosun University

We have investigated ultra-narrow EIA spectral features with respect to variations of polarizations and powers of pump laser beam in a degenerate two-level system of the transition $F_g = 3 \rightarrow F_e = 4$ of ^{85}Rb D_2 transition line $\left(5S_{1/2} \rightarrow 5P_{3/2}\right)$. Polarizations of the probe laser beam in two separate experiments were fixed at right circular and horizontal linear polarizations, respectively while the polarizations of the pump lasers were varied from initial polarizations same as the probe laser beams to orthogonal to probe polarizations. In the circular polarization experiment, the pump polarization was varied from right circular polarization to left circular polarization through a linear polarization. In the linear polarization experiment, the pump polarization were varied from vertical polarization to horizontal polarization by rotating the vertical linear polarization. One homemade laser combined with AOMs was used to the pump and probe laser beams instead of two different lasers to overcome broad linewidths of the homemade lasers. Theoretically, ultra-narrow EIA spectra were obtained from probe absorption

coefficient calculated from optical Bloch equations of the degenerate two level system prepared by a pump laser beam.

In the case of the circular polarization, EIA signal was obtained as expected theoretically although both pump and probe beams have same polarization. The EIA signal become smaller as power increases and polarizations of the pump and probe beams were same. When the polarization of the pump beam was linear polarization, maximum EIA signal was obtained theoretically and experimentally. Experimental EIA spectral shapes with respect to variations of the pump beam polarization shows similar trends as the theoretical results.

Chapter 1

1. Introduction to EIA and EIT

1.1. Background

Recently quantum coherence techniques have been used to manipulate quantum states using coherent lasers, which enhance or decrease the populations of a specific state. In quantum optics community, electromagnetically induced absorption (EIA) or electromagnetically induced transparency (EIT) have been investigated for the applications such as quantum information processing, gravitational wave detection, high resolution spectroscopy, tight locking of laser to optical transitions, lasing without inversion (LWI), generate ultra-slow optical solitons, four wave mixing process, atomic clock, atomic magnetometers, quantum teleportation [1-4]. Sub-natural spectral linewidths of EIA and EIT have made such applications possible.

At least three-state of atoms or molecules interacting with two coherent optical fields should be prepared to have such quantum interference phenomena. The three-state can be categorized as V–configuration, Ladder configuration and Λ–configuration as shown in Fig. 1.

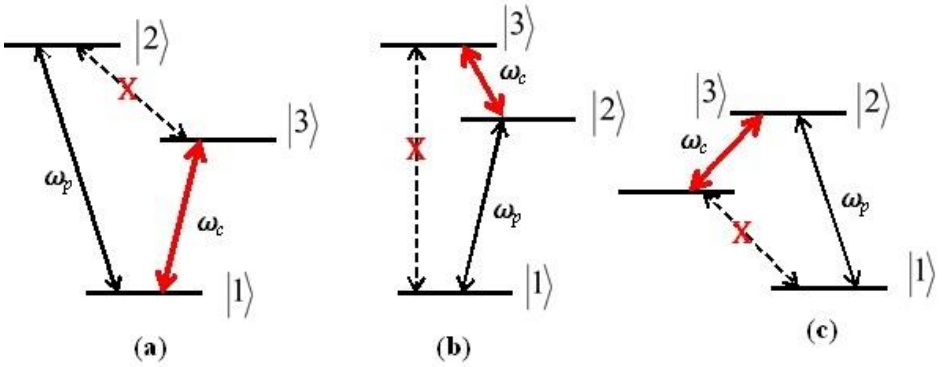

Fig. 1.1 Different three-level atomic levels configuration schemes for EIT and EIA. (a) V configuration (b) Ladder configuration, (c) Λ configuration

The EIT and EIA have also been explained using V and Λ type of connections between two levels in the degenerate two-level system. The degenerate two-level system is composed of many V and Λ types due to many magnetic sublevels of the degenerate two-level system instead of three-level system.

Polarizations of the pump and probe laser beams in the degenerate two level system play roles in Zeeman coherences of the ground and excited states, transfer of the coherence from the excited states, contribution to optical coherences between the ground and excited states because the polarizations connect magnetic sublevels of the ground state with those of the excited states. Depending on the cases of the polarizations of the pump and probe lasers, trapping of the sublevels of the ground state can occur or not so that EIA or EIT can be formed.

In our group EIA with ultra-narrow EIA signals have been investigated from such degenerate two-level system in rubidium atom. However, still polarizations of pump and probe lasers were confined in special same and

orthogonal cases of the pump and probe lasers. Previous other investigations of the spectra of the EIA and EIT have also been done using restricted parameters in a specific polarization and laser intensities because including many parameters such as arbitrary polarizations, power, time dependences of the atom, etc. makes it difficult to solve the solutions of the system.

In this work we extend polarization dependences of EIA signal to more general cases, where the maximum ellipticity between the probe and pump beam i.e., $\left(\sigma^{+}-\sigma^{-}\right)$ for circular and $\left(\pi \perp \pi\right)$ for linear polarization case have been applied by keeping the probe beam ellipticity fixed and changing pump beam's ellipticity by ε=15 until both beams achieve same polarization $\left(\sigma^{+}-\sigma^{+}\right)$ for circular and $\left(\pi \| \pi\right)$ linear polarization case.

1.1.1. Recapitulation of previous work

In the EIA experiment there are pump and probe lasers beams. One probe beam probes the system while the second pump beam prepares state of system. There are two ways to probe the atomic system to investigate EIA spectral profiles. (i) Two independent pump and probe laser sources can be used. (ii) And to use a single laser source combined with AOMs is more fantastic way to probe ultra-narrow EIA signals below sub-natural line profiles because phase noises between two independent lasers can be removed and scanning resolution of the spectral line profile is dependent on resolution of AOM scanning independent of relative phase shift and linewidth differently from case of two independent laser cases. The second case has been implemented nicely in our lab.

In optical pumping of atoms the coherent population trapping (CPT) which can be produced in three-level atomic system interacting with two coherent laser fields is one of the most interesting coherent effects. CPT was first observed by Alzetta *et al.* [6]. Generally in CPT two ground hyperfine levels of alkali atoms are coupled to a common excited level i.e., Λ configuration as shown in Fig. 1.1. When the difference between frequencies of probe and pump beams is equal to the difference of frequencies of two ground levels, and then atoms are prepared in a non-absorbing state [5]. This non-absorbing state refers as "dark state" of an atom or molecule that cannot absorb photons.

CPT is a spectroscopic phenomenon which involves only modifications to the material states in an optically thin sample. In contrast to CPT, EIT is an occurrence specific to the optically thick media where both the optical fields and the material states are modified. The cause of the modified optical response of an atomic medium in this case is the laser induced coherence of the atomic states which leads to quantum interference was first reported by Harris *et al.* [7] using probe and pump beam in co-propagating direction with right circular (σ^+) polarization for both beams. The probe transmission gets apparently transparent when the coupling (pump) laser is tuned to the line center of $5s5p\,^1P_1 - 4d5d\,^1D_2$ transition. In this experiment they point out two physical informative ways that can view EIT. (i) the picture that arises from the work of [7] where the dressed states can be viewed as simply comprising two closely spaced resonances effectively decaying to the same continuum [7, 20], (ii) The picture of EIT can be seen as arising through different pathways between the bare states. The effect of the fields is to transfer small, but finite amplitude.

More reviews and specific aspects of EIT like dependence of EIT on different parameters and its application can be found in Lukin *et al.* [8], Matsko *et al.* [9], and Vitanov *et al.* [10].

Bo Gao [22, 23] gives an analytical solution of the steady-state density matrix for two-level atoms with arbitrary ground state the polarization of lasers are linearly (π). Also he observed the probe spectra for closed Zeeman degenerate two-level system (DTLS) of Cesium atoms. Through this he develops a method for calculating the weak probe absorption by closed DTLS with linearly polarized pump beam in the absence of magnetic field.

Interestingly, the first EIA experimental occurrence was in 1998 by A.M. Akulshin *et al.* [12], then afterward in 1999 theoretical explanation of physical origins of EIA was given by A. V. Taichenachev *et al.* [11, 29] by using a simple analytically tractable model of a four-level *N*-configuration system.

Shigeru Nagayama [24] gives a theoretical analysis of the Doppler-free signals in saturation spectroscopy, polarization spectroscopy and mixing of saturation and polarization spectroscopies in four-level system. For analyzing Doppler free signals he [24] uses different combination of probe and pump polarization which termed as circular optical anisotropy and linear optical anisotropy of atom with material susceptibility χ . In circular optical anisotropy calculation shows the difference produced in absorption coefficient and refractive index when pump and probe beams are left $\left(\sigma^{-}\right)$ and right $\left(\sigma^{+}\right)$ circularly polarized. Similarly, for linear optical anisotropy the difference occur in absorption coefficient and refractive index between linear and circular beams $\left(\pi \text{ and } \sigma^{\pm}\right)$.

EIA is explained as spontaneous transfer of the atomic coherence (TOC) or population difference (TOP) induced in an excited state to the ground state level of an atom. EIA media is quite different from EIT media, not only because of the positive sign of the resonance in EIA and negative resonance in EIT [11] but non-linear magneto-optical polarization rotation has opposite sign in EIA and EIT medium. Group velocity of light in EIT medium can be much smaller than the speed of light because of normal dispersion near EIT resonance, while in EIA there is an abnormal dispersion near resonance which leads to fast or subluminal light. Akulshin *et al.* [12] stated first experimental observation of increasing absorption and fluorescence for upper ground state hyperfine level (GSWL) of rubidium vapor cell. Moreover, [12] explained that with various polarization combination of pump and probe beams different energy-level configurations can achieve. For example, with left $\left(\sigma^{-}\right)$ and right $\left(\sigma^{+}\right)$ circular polarization of pump and probe beam one can attain lambda $\left(\Lambda\right)$ configuration. And if the polarization combination applies to multi Zeeman sublevels with the condition of $\left[\left(2F+1\right)\geq\left(2F'+1\right)\right]$ CPT can take place. Or if the polarization of probe and pump beams are same $\left(\sigma^{+}-\sigma^{+},\sigma^{-}-\sigma^{-},\pi-\pi\right)$ than result will be in superposition of two-level systems. Furthermore, Lezama *et al.* [13] explore and define EIA in a DTLS with same experimental setup explained in [12] and also state three conditions for EIA: (i) relationship between ground $\left(F_g\right)$ and excited $\left(F_e\right)$ states hyperfine quantum number must be $F_g \rightarrow F_e = F_g + 1$ (ii) ground state should be degenerate $\left(F_g > 0\right)$ to allow long-lived Zeeman coherence lastly (iii) system must be closed.

Lezama *et al.* [14, 15] gives detail evidence both theoretically and experimentally for the absorption spectra in specially EIA which is not appear in three-level configurations. In [14] Lezama *et al.* discussed the probe absorption spectra with respect to polarization of probe and pump beam in a closed and open transitions. In [15] they used rubidium atomic beam to reduce Doppler broadening and observed absorption spectra for $F_g = 3 \rightarrow F_e = 4$ transition of ^{85}Rb with four different polarization combination of probe and pump beams $\left(\sigma^+ - \sigma^+, \pi \| \pi, \sigma^+ - \sigma^-, \pi \perp \pi\right)$. Which conclude, that whenever probe and pump beams have same polarization $\left(\sigma^+ - \sigma^+, \pi \| \pi\right)$ the EIA peak is small and EIA peak gets prominent with perpendicular polarization $\left(\sigma^+ - \sigma^-, \pi \perp \pi\right)$ of probe and pump beams.

C. Goren *et al.* [18] explain the occurrence of EIA for the transition of $F_e = F_g + 1$ and $F_g > 1$ in the case of same polarization of probe and pump beam. Furthermore, Goren *et al.* explain that EIA was due to the TOP and called it EIA-TOP. In [18], Goren *et al.* used double two-level system (TLS) which was equivalent to four-state *N*-configuration system. In each model Doppler broadening increases the width of dip. In double TLS EIA peak become narrower on Doppler broadening but it contradict with N-type system. For the closed transition $F_g = 2 \rightarrow F_e = 3$ of ^{87}Rb, with circular and linear polarizations of probe and pump respectively then EIA occurred due to TOC and if both have linear polarizations then the EIA occurs due to TOP.

There was much theoretical work which shows that EIA can be occurred in an open system but experimental work was present by S. K. Kim *et al.* [16]. Kim *et al.* observed absorption spectra in open systems of ^{85}Rb D_1,

^{87}Rb D_1 and D_2 transition lines in which probe and pump beams were co-propagating. Furthermore, spontaneous TOC in [14] was not able to explain the standard EIA in an open system, therefore Chou *et al.* [17] gave dressed atom multiphoton spectroscopy (DAMS) that provide a clear interpretation for EIA. Chou *et al*. explained that EIA occurred from quantum interference among competing multiphoton pathways which they called *anomalous EIA*.

C. Goren *et al.* [28] shown that TOC effect the whole system and with increasing power of pump beam the EIA peak splits. Moreover, they shown that if pump polarization was right circular $\left(\sigma^{+}\right)$ and probe was linearly $\left(\pi\right)$ polarized, then the results of *N*-configuration were exactly same as in realistic systems.

Taichenachev *et al.* [11] describe a sign for EIA resonance for the experiment in [12] and also explain the EIA theoretically in terms of TOC for perpendicular polarization combination in four-state N-configuration atoms. In another experiment C. Goren *et al.* [19] achieved EIA via TOP as well as TOC at very low power of pump laser beam and give EIA peak at the center. Furthermore, T. Zigdon *et al.* [20] performed an experiment for rubidium atoms for the transition of $F_g = 2 \rightarrow F_e = 3\left(F_g \rightarrow F_e = F_g + 1\right)$ ^{87}Rb atoms in which probe beam is stronger than the pump beam with opposite circular polarization then at center a sharp dip arise which was called transparency within transparency (TWT). Furthermore, T. Zigdon *et al.* [30] study the effect of strong probe beam on the absorption of pump beam with conclusion that with circular (left or right) polarization of pump beam and linear polarization of probe or vice versa, the probe beam absorption extremely depend upon the Zeeman coherences between the nearest Zeeman level (ground/excited) and if both beams are opposite circularly polarized then

Zeeman coherence determine that the absorption were between next to neighboring levels.

M. Kwon *et al.* [25] observed EIA in Cs atomic vapor cell for D_2 $F_g = 4 \rightarrow F_e = 5$ transition at room temperature. In this experiment, Kwon *et al.* used both two independent lasers and one laser source for probe and coupling (pump) beams. By doing experiment [25] with single laser, high mutual coherence can achieved which results the EIA spectra become much narrower than $0.1\ \Gamma$ on the weak coupling field. The total bandwidth of EIA around the transparent resonance was very narrower than the natural bandwidth of 5.3 MHz. In another experiment A. M. Akulshin *et al.* [26] used a single extended cavity diode laser (ECDL) for both probe and pump beams which were co-propagating through the Cs vapor cell D_2 line to study the atomic medium with steep and sign-reversible dispersion.

Alzetta *et al.* [5] used linear and circular polarized pump and probe beam in rubidium D_1 and D_2 lines. In which EIA peaks were observed in Hanle experiment for an open system for the very first time. Alzetta *et al.* observed dark resonance for the transition of $F_g \rightarrow F_e = F_g - 1$ and $F_g \rightarrow F_e = F_g$ but bright resonance also observed for the transition of $F_g \rightarrow F_e = F_g + 1$ with the linear polarization of laser beam. But if the polarization of laser beam changes to circular polarization then the condition for dark and bright resonance reversed (except $F_g = 2 \rightarrow F_e = 3$ ^{85}Rb D_1 line) similar type of result were found for Cesium vapor cell by Andreeva *et al.* [27]

In experiments, conversion from EIA to EIT or EIT to EIA was presented by K. Dahl *et al*. [31] in which the pump laser absorption profile for four different polarization configurations in DTLS of Cs atom. In case of circular

and orthogonal polarization of pump and probe beams, the absorption within transparency and transparency within transparency were detected when the power of probe laser exceeded from power of pump beam. Absorption with in transparency was observed in case of linear and circular polarization combination of pump and probe laser fields.

Hafeez *et al.* [32] explain EIA spectra theoretically as well experimentally for $F_g = 3 \rightarrow F_e = 4$ transition for ^{85}Rb atoms with same and orthogonal circular polarizations $\left(\sigma^+ - \sigma^+, \sigma^- - \sigma^+\right)$ of probe and pump beam for both cold and thermal rubidium atoms. Hafeez *et al.* shows that for same polarization $\left(\sigma^+ - \sigma^+\right)$ EIA not occurred for low power of coupling laser. But for orthogonal polarization $\left(\sigma^- - \sigma^+\right)$ the EIA splits (theoretically) but in experiment data no split of EIA observed because the linewidth of center peak is around 1 MHz and the two independent lasers have broad linewidth.

Chapter 2

2. Spectroscopic characteristics of rubidium atoms interacting with laser beams

2.1. Basic information of rubidium

2.1.1. Introduction

Rubidium is an element with symbol Rb and atomic number 37. Rubidium is a soft, silver-white alkaline metallic element in IA group of the periodic table with the ground state electronic configuration of $1s^2$, $2s^2$, $2p^6$, $3s^2$, $3p^6$, $4s^2$, $3d^{10}$, $4p^6$, $5s^1$. The next higher energy configuration has the 5s valence electron promoted to a 5*p* orbital with no change in the description of the remaining 36 electrons. Natural rubidium has two different isotopes: ^{85}Rb is present to the extent of 72% while ^{87}Rb constitutes the remaining 28% of abundance.

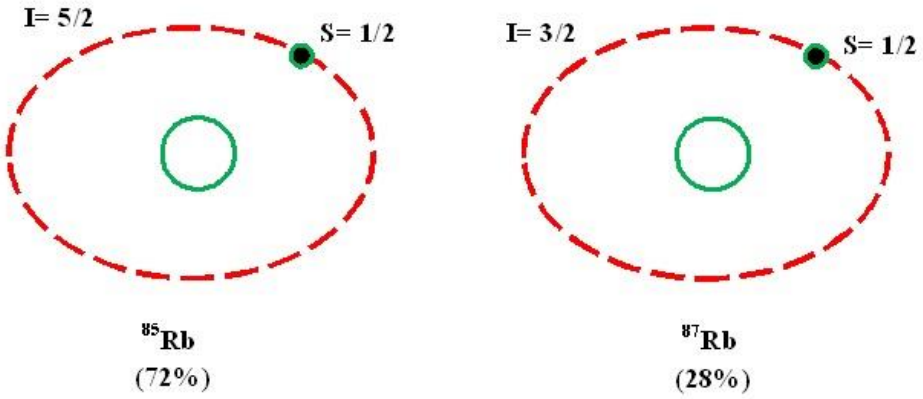

Fig. 2.1 Two different isotopes of rubidium atoms found in nature, ^{85}Rb and ^{87}Rb. Both have only one valence electron but a major difference between them is in the nuclear spin *I*.

2.1.2. Energy levels in rubidium

One valence electron atom such as Rb atom that neglects both the electron and nuclear spins can be treated as central field approximation (CFA). In CFA, quantum numbers for atomic configuration are described as:

(a) Principal quantum number n should be greater than *zero* $(n > 0)$.

(b) Orbital angular quantum number l should be from *zero* to $(n-l)$.

$(0 \le l \le (n-l))$.

(c) Magnetic quantum number m_l ranges from $-l$ to l $(-l \le m_l \le l)$.

(d) Electron spin quantum number s has only value ½. $\left(s = \frac{1}{2}\right)$.

(e) Only allowed values of spin projection quantum number m_s are

$$\pm \frac{1}{2} \quad \left(m_s = \pm \frac{1}{2}\right).$$

The spinless model plays a vital role in the low-resolution spectrometer to observed transmission and absorption spectra of rubidium. However,

higher resolution for instruments like the apparatus we used in our lab CFA cannot explain phenomenon completely. There are three drawbacks; (i) CFA does not take account of spin of the electron (ii) and of the nucleus and (iii) the additional magnetic field.

2.1.3. Fine structures splitting

The spin of the electron is important because it couples with the orbital angular momentum. Specially, the electron feels an effective magnetic field as it moves through the electrostatic field of nucleus (Coulomb's force). Since the electron has an intrinsic magnetic moment due to its spin, its energy level is higher if it is aligned opposite to the effective magnetic field than if it is aligned with it. Only the states with non-zero orbital angular momentum are affected, and the net result is that they are split into multiple levels due to external fields, depending upon the orientation of the spin. This is known as fine-structure splitting.

Once we take electron spin into consideration, we modify our spectroscopic notation known as Russel-Saunders notation. This introduces new quantum numbers:

(a) L describing the magnitude of total orbital angular momentum.

$$L = \sum l_i \tag{2.1}$$

Allowed value of L is 0, 1, and 2.

(b) S describing the magnitude of total electron spin angular momentum.

$$S = \sum s_i \tag{2.2}$$

(c) J describing the magnitude of total electron angular momentum.

$$J = L + S \tag{2.3}$$

Allowed value of J ranges from $|L-S|$ *to* $|L+S|$.

Each state is labeled by term symbol ${}^{(2S+1)}L_J$ and the energy quantum number n is dropped. The orbital angular momentum is again labeled with old spectroscopic letters (S, P, D, *etc.*), but this time in capital form.

2.1.4. Hyperfine structure levels

According to [40], adding up nuclear spin I introduces three additional terms to the Hamiltonian, each of which is related to the nuclear magnetic moment associated with I. The electron's orbital angular momentum, the electron's spin and the nuclear spin all are added up to a total angular momentum,

$$F = I + J \tag{2.4}$$

with following different F values,

$$|I-J| < F < |I+J|$$

Each F has a slightly different energy due to the coupling between the electron and the nucleus' intrinsic magnetic field. Finally, if external magnetic field is applied, then F further splits because the energy of the system is different for different orientations of the atom called the *Zeeman Effect*. The difference between Zeeman Effect and hyperfine splitting is that in Zeeman Effect magnetic field is due to the magnetic field we apply in the lab while hyperfine splitting is due to the intrinsic magnetic field that occurs inside the atom itself. Detail description of fine and hyperfine structures of ^{85}Rb and ^{87}Rb are described in Appendix A.

2.1.5. Interaction of rubidium atom with laser beams

For the interaction of rubidium atom with a laser beam, we consider ^{87}Rb isotope. For understanding, [41] the dipole allowed transition interaction of rubidium atom with a laser beam between two relevant eigenstates, we consider an operator $\left|\vec{d}.\hat{\varepsilon}_q\right|$, where $\vec{d}$ is the dipole moment, $\hat{\varepsilon}$ is the electric field of the laser beam and q represents the different polarizations of the laser light.

q value	Polarization of light
q = -1	σ^- (left circular polarization)
q = +1	σ^+ (right circular polarization)
q = 0	π (linear polarization)

Table 2.1 q values for different polarizations of laser beam.

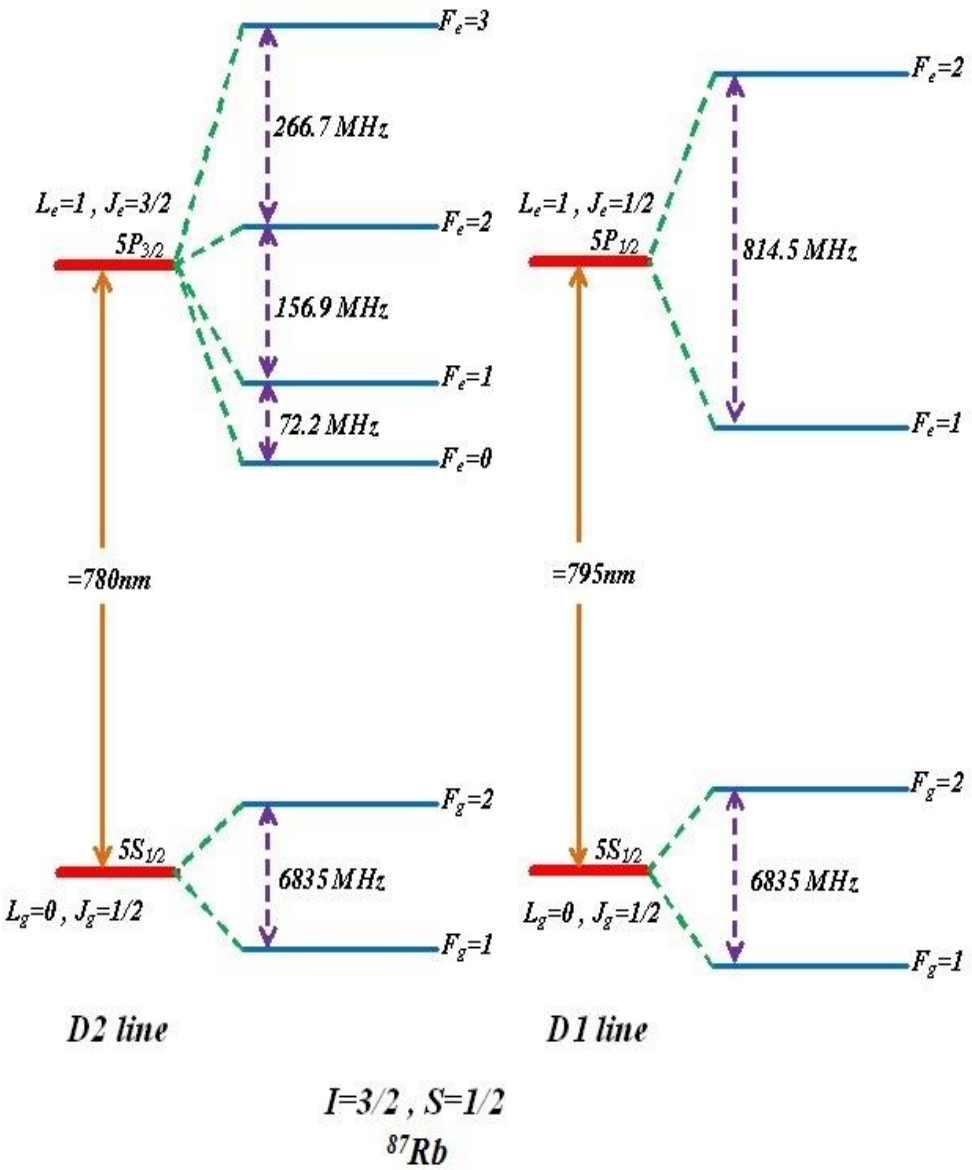

Fig. 2.2 Energy level diagram of the ^{87}Rb D_2 and D_1 line hyperfine splitting with the value of *I* and *S* for ^{87}Rb. *L* and *J* values for each fine structure level of ground and excited states are shown.

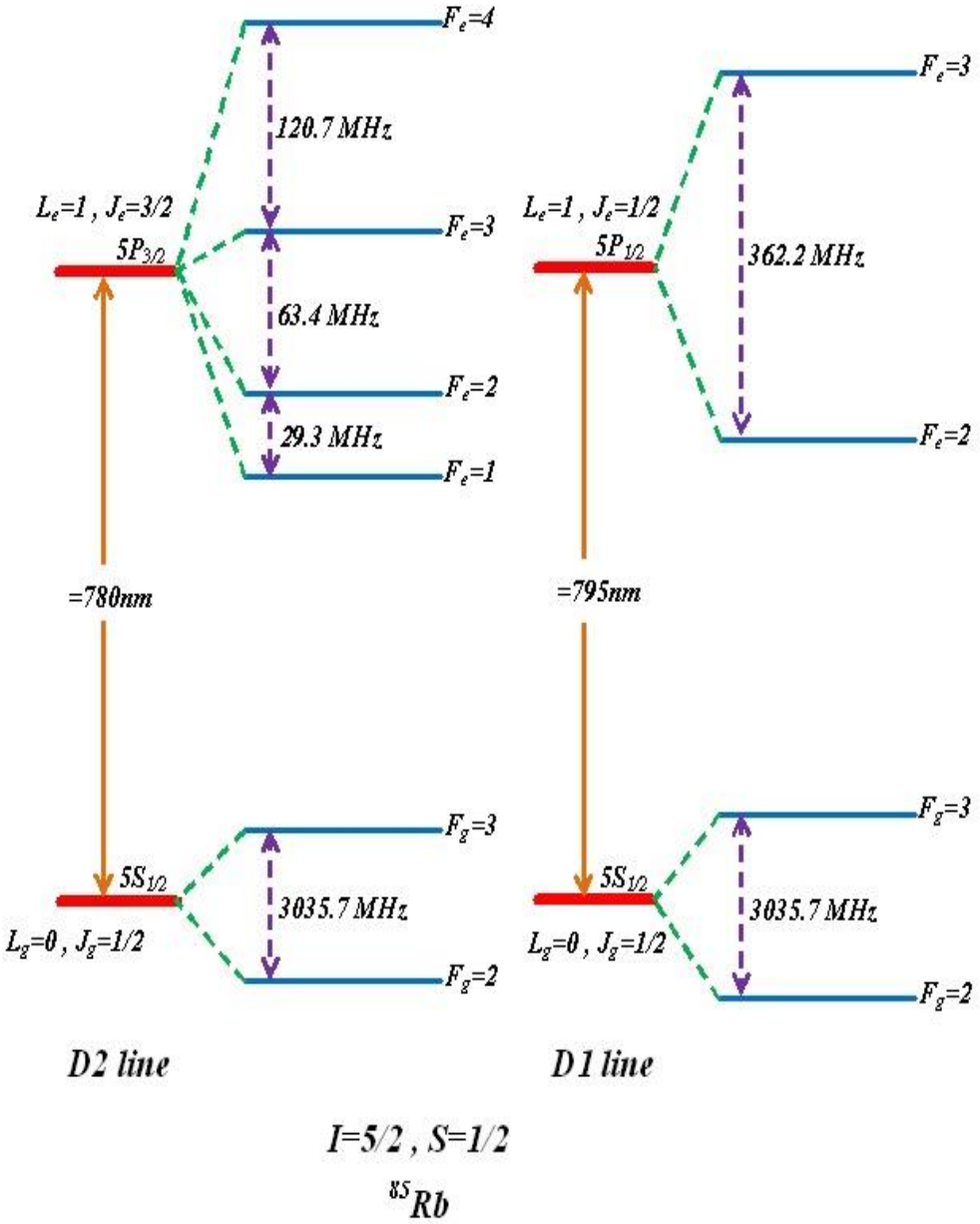

Fig. 2.3 Energy level diagram of the ^{85}Rb D_2 and D_1 line hyperfine splitting with the value of *I* and *S* for ^{85}Rb. *L* and *J* values for each fine structure level of ground and excited states are shown.

The interaction of laser beam between the excited state $|F_e, m_e\rangle$ and $|F_g, m_g\rangle$ the ground state is given by,

$$\left\langle F_e, m_e \left| \vec{d}.\hat{\varepsilon}_q \right| F_g, m_g \right\rangle = (-1)^{F_e - m_{F_e}} \begin{pmatrix} F_e & 1 & F_g \\ -m_{F_e} & q & m_{F_g} \end{pmatrix} \left\langle F_e \left\| \vec{d} \right\| F_g \right\rangle \quad (2.5)$$

where $\begin{pmatrix} F_e & 1 & F_g \\ -m_{F_e} & q & m_{F_g} \end{pmatrix}$ is *3J* value.

Using Wigner-Eckart Theorem, $\left\langle F_e \left\| \vec{d} \right\| F_g \right\rangle$ is derived as followings,

$$\vec{J} + \vec{I} = \vec{F}$$

$$\left\langle F_e \left\| \vec{d} \right\| F_g \right\rangle = \left\langle J_e I F_e \left\| \vec{d} \right\| J_g I F_g \right\rangle$$

$$\left\langle F_e \left\| \vec{d} \right\| F_g \right\rangle = (-1)^{F_e + I + J_e + 1} \sqrt{(2F_e + 1)(2F_g + 1)} \begin{Bmatrix} J_e & 1 & J_g \\ F_g & I & F_e \end{Bmatrix} \left\langle J_e \left\| \vec{d} \right\| J_g \right\rangle, \quad (2.6)$$

where $\begin{Bmatrix} J_e & 1 & J_g \\ F_g & I & F_e \end{Bmatrix}$ is *6J* value.

The relations between orbital angular momentum, spin angular momentum, and total angular momentum is from equation (2.4) in vector form,

$$\vec{L} + \vec{S} = \vec{J}$$

In equation (2.6) $\left\langle J_e \left\| \vec{d} \right\| J_g \right\rangle$ is equal to,

$$\left\langle J_e \left\| \vec{d} \right\| J_g \right\rangle = \left\langle L_e S J_e \left\| \vec{d} \right\| L_g S J_g \right\rangle$$

$$\left\langle J_e \left\| \vec{d} \right\| J_g \right\rangle = (-1)^{J_g + L_e + S + 1} \sqrt{(2J_e + 1)(2J_g + 1)} \begin{Bmatrix} L_e & 1 & L_g \\ J_g & S & J_e \end{Bmatrix} \left\langle L_e \left\| \vec{d} \right\| L_g \right\rangle, \tag{2.7}$$

where $\begin{Bmatrix} L_e & 1 & L_g \\ J_g & S & J_e \end{Bmatrix}$ is 6J value.

Substituting equations (2.6) and (2.7) in equation (2.5), we get

$$\begin{aligned} \left\langle F_e, m_{F_e} \left| \vec{d}.\hat{\varepsilon}_q \right| F_g, m_{F_g} \right\rangle &= (-1)^{2F_e + I + 2J_g + L_e + S - m_{F_e}} \left\langle L_e \left\| \vec{d} \right\| L_g \right\rangle \\ &\times \sqrt{(2F_g + 1)(2F_e + 1)(2J_g + 1)(2J_e + 1)} \\ &\times \begin{Bmatrix} L_e & 1 & L_g \\ J_g & S & J_e \end{Bmatrix} \begin{Bmatrix} J_e & 1 & J_g \\ F_g & I & F_e \end{Bmatrix} \begin{Bmatrix} F_e & 1 & F_g \\ -m_{F_e} & q & m_{F_g} \end{Bmatrix} \end{aligned}$$

or,

$$\begin{aligned} C_{F_e, m_{F_e}}^{F_g, m_{F_g}} &= (-1)^{2F_e + I + 2J_g + L_e + S - m_{F_e}} \\ &\times \sqrt{(2L_e + 1)(2F_g + 1)(2F_e + 1)(2J_g + 1)(2J_e + 1)} \\ &\times \begin{Bmatrix} L_e & 1 & L_g \\ J_g & S & J_e \end{Bmatrix} \begin{Bmatrix} J_e & 1 & J_g \\ F_g & I & F_e \end{Bmatrix} \begin{Bmatrix} F_e & 1 & F_g \\ -m_{F_e} & q & m_{F_g} \end{Bmatrix} \end{aligned} \tag{2.8}$$

Here $C_{F_e, m_e}^{F_g, m_g}$ is called the Clebsch-Gordan coefficients which represent the relative transition strengths. Fig. 2.5 shows the square of the Clebsch-Gordan coefficients for ^{85}Rb. Relative transition strengths from those Clebsch-Gordan coefficients between the excited and ground states of Rb atoms are shown in Fig. 2.4. Real relative strengths between the different transitions from those Clebsch-Gordan coefficients and the decay rate of the excited state Γ can be derived.

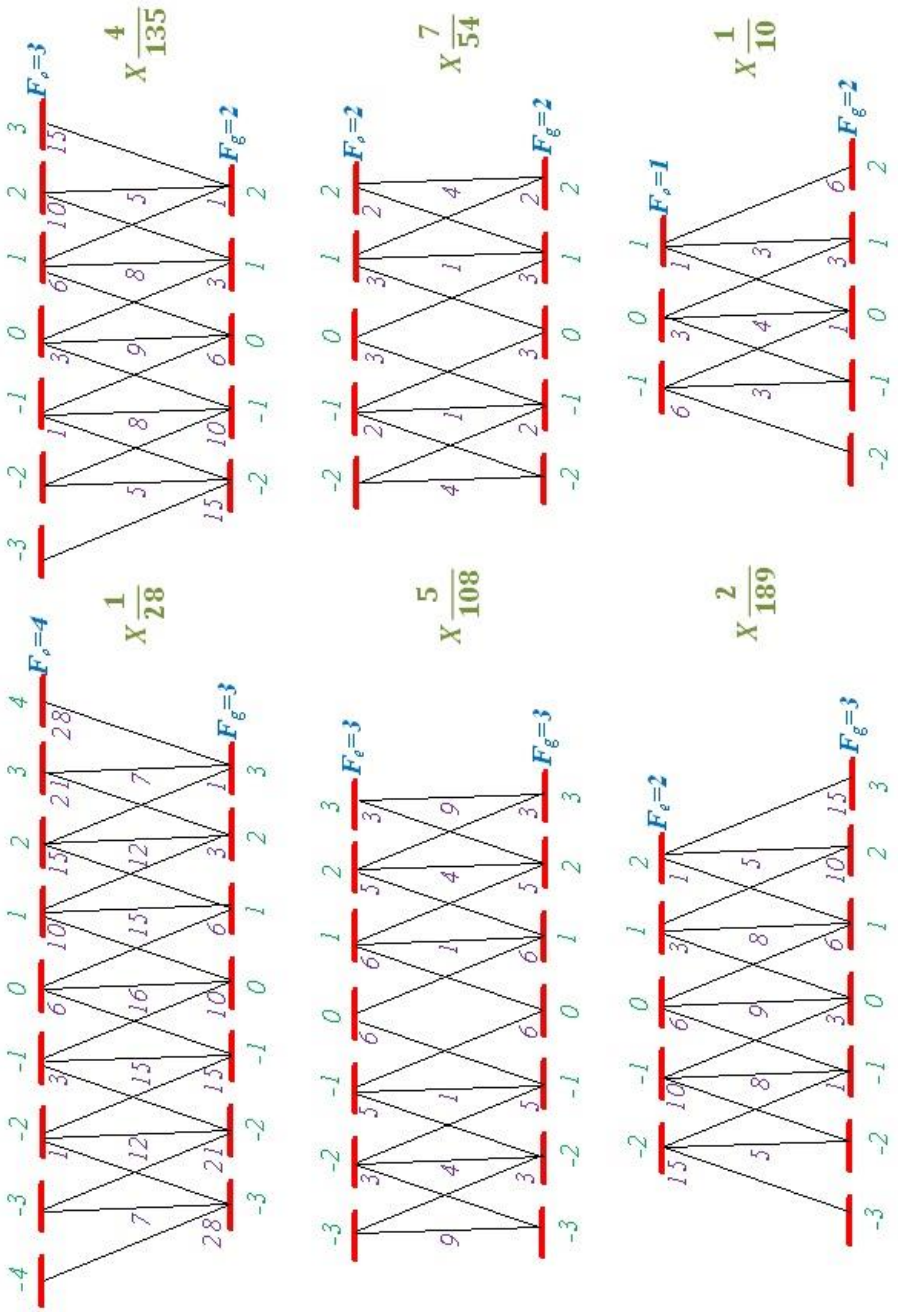

Fig 2.4 The relative transition strengths between the excited and ground states of Rb atoms. [42]

2.2. Saturation absorption spectroscopy (SAS) of rubidium

2.2.1. A brief history of modern laser spectroscopy

Modern laser spectroscopy began with the invention of the laser, which provides intense, collimated monochromatic radiation throughout optical spectral range. A laser beam with its high intensity, narrow spectral linewidth, and phase coherence opened the field of ultra-high resolution spectroscopy in atomic and molecular laser community. Linewidths of such atomic and molecular spectroscopic lines were limited due to Doppler broadening of fast moving thermal atoms and molecules. Saturation spectroscopy developed by Javan, Schawlow, W. E. Lamb, Jr. and others, provided sub-Doppler resolution of spectral lines of atom and molecules in gaseous states. Intense, monochromatic laser light can selectively saturate an optical transition, producing extremely narrow Doppler-free resonances. Atomic beams were also used to eliminate Doppler broadening and produce narrow spectral lines. Investigation on the spectral shapes of these narrow lines reveals very important collisional processes, etc. of atoms and molecules. Further, by locking the laser frequency to this narrow spectral line, its wavelength could be accurately confirmed. These techniques make possible laser wavelength and frequency standards, etc.

2.2.2. Doppler broadening effects on atoms

Thermal motions of atoms or molecules in gaseous state bring Doppler broadening or shifts of atomic and molecular absorption and emission spectral lines depending on the atomic and molecular velocities. Saturation

absorption spectroscopy (SAS) is a technique used for resolving very fine spectral splitting of hyperfine structures in atomic spectra.

If an atom is moving toward or away from a laser beam wavevector (***k***), then the atom sees blue or red detuned laser frequency due to Doppler effects, respectively. If an atom is at rest, relative to the laser beam, absorbs laser photons with frequency ν_0, then when the atom is approaching to direction of the laser wavevector, the atom sees blue-shifted radiation, thus the laser frequency for absorption must be less than ν_0 because atom sees blue-shifted laser frequency to the resonance value of ν_0. Similarly, for the atom moving opposite to the direction of the laser wavevector, the laser frequency must be greater than ν_0 for absorption to occur. If the atom is moving along the z axis, relative to the laser wavevector with $v_z << c$, then the frequency of the absorbed radiation in the rest frame of the atom is ν_L;

$$\nu_L = \nu_0 \left(1 + \frac{v_z}{c} \right) \tag{2.9}$$

If v_z is negative (motion toward the laser), then $\nu_L < \nu_0$, that is, the atom moving toward the laser will absorb radiation that is blue-shifted from ν_L up to ν_0. And if v_z is positive (motion away from the laser) then $\nu_L > \nu_0$ i.e., the atom absorbs radiation that is red-shifted from ν_L down to ν_0. Therefore, atoms having a distribution of speeds absorb laser photons over a range of frequencies.

The probability that an atom has a velocity between v_z and $v_z + dv_z$ is given by the Maxwell distribution,

$$P(v_z)\,\mathrm{d}v_z = \left(\frac{M}{2\pi kT}\right)^{\frac{1}{2}} \exp\left(-\frac{Mv_z^{\,2}}{2kT}\right) dv_z \tag{2.10}$$

where M, k and T are mass of an atom, Boltzmann constant, and absolute environmental temperature, respectively. Then equation (2.9) becomes,

$$v_z = (\nu_L - \nu_0)\frac{c}{\nu_0}$$

$$dv_z = \frac{c}{\nu_0} d\nu_L \tag{2.11}$$

By solving equations (2.12) and (2.13),

$$P(v_z)dv_z = \frac{2}{\pi\delta^{1/2}} \exp\left[-\frac{4(\nu_L - \nu_0)^2}{\delta^2}\right] d\nu_L, \tag{2.12}$$

where δ is linewidth parameter

$$\delta = 2\left(\frac{\nu_0}{c}\right)\left(\frac{2kT}{M}\right)^{1/2}$$

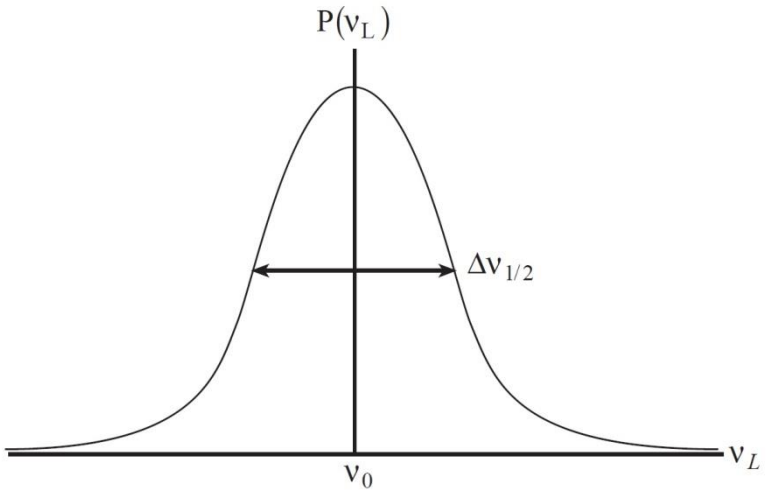

Fig. 2.5 Doppler broadening spectral line, where $\Delta\nu_{1/2}$ is the FWHM and ν_0 is the absorbed frequency when atom is at rest in the frame of the laser.

2.2.3. Doppler-free saturation absorption spectroscopy

The experimental setup for the saturation absorption spectroscopy [33, 34] is a schematically demonstrated in Fig. 2.7. The output beam from the laser is split into three beams, two less intense probe and pump beams and a more intense beam for further experimental setup of ultra-narrow EIA, at the thick beamsplitter. One beam, reflected at the back surface is used as a probe beam while the second reflected from the front surface is used as pumping laser. After being reflected twice by mirrors, the more intense pump beam passes through the rubidium cell from left to right while pump beam reflected from mirror entering into a cell from right to left named counter propagating. Inside the rubidium cell there is a region of space where the pump and a probe beam overlap and, hence, interact with the same atoms. The beam size of each beam is about 3 mm.

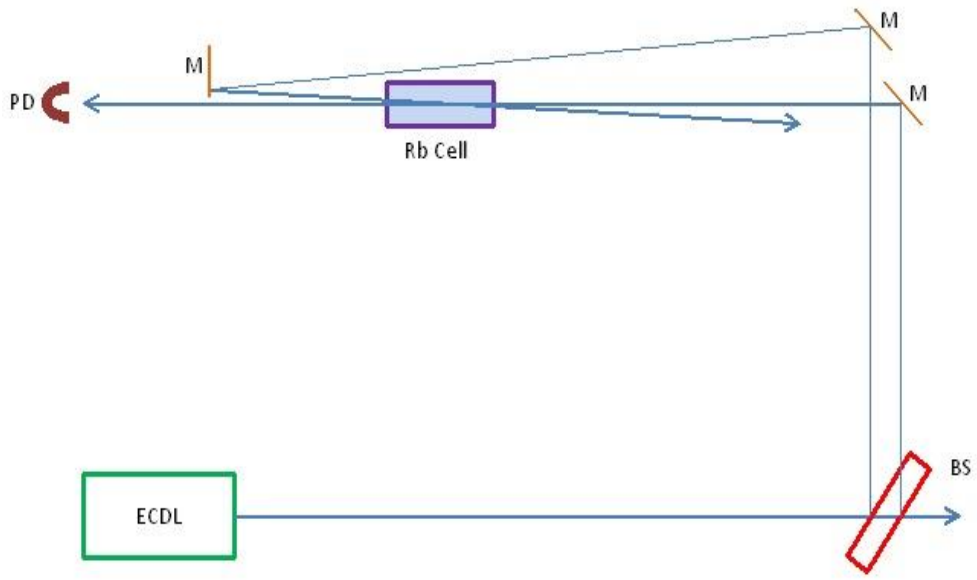

Fig. 2.6 Experimental setup for saturation absorption spectroscopy.

The pump beam changes the populations of the atomic ground states and the probe detects these changes. Considering how the pump beam changes the populations, we know how these changes affect to the probe signal. As discussed above, due to the Doppler shift, only atoms with a particular velocity v_z are in resonance with the pump beam frequency, and thereby be excited. At the same time the absorption of probe beam decrease when the beam interacts with those same velocity group of atoms. The velocity component along the laser beams vanishes, this Doppler free resonance occurs and detected by photodiode. Very narrow spectral lines of SAS signals are used to stabilize the frequency of laser.

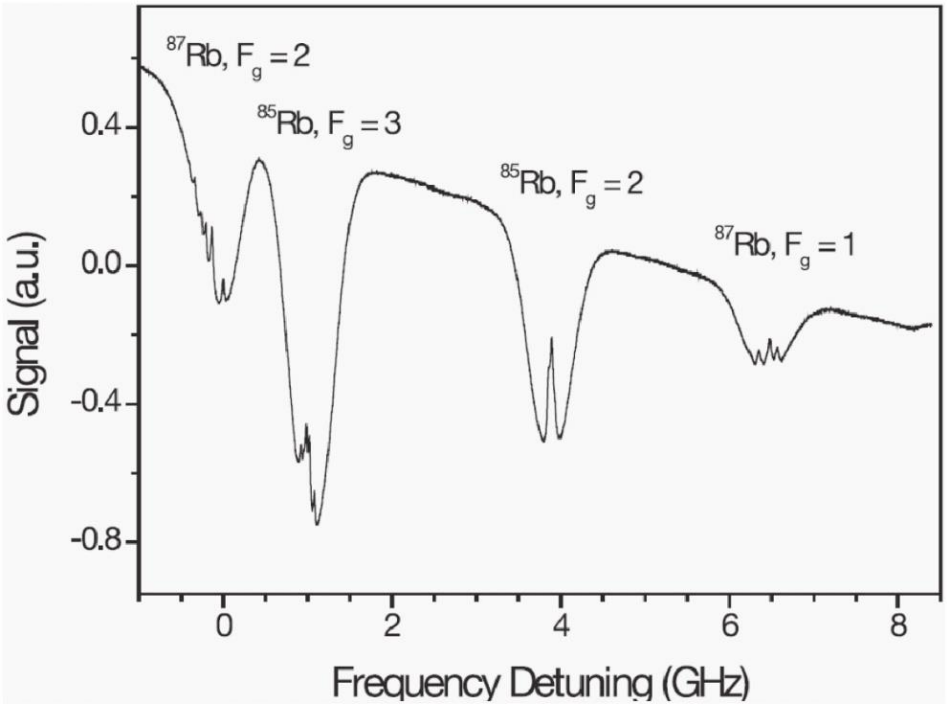

Fig. 2.7 Saturation absorption spectra for ^{85}Rb and ^{87}Rb for D_2 transition line [44].

Fig. 2.7 shows observed SAS spectra of ^{85}Rb and ^{87}Rb for D_2 transition line. Extra crossover peaks occur in SAS signals of rubidium, other than three peaks due to transition from one level to another. They arise whenever there are enough atoms whose Doppler shifts are exactly half the frequency difference between two transitions. Because the pump and probe beams are counter propagating, the atom sees them Doppler shifted by equal and opposite amounts. If the laser frequency in the lab rest frame is exactly halfway between the two transitions, the atom will experience both pump and probe as being on resonance. A technique suggests by V. Natarajan *et al.* [35] to eliminate the extra peaks i.e., crossover from the saturated absorption

spectra by using the pump and probe beam moving in the same direction (co-propagating) through the cell.

Chapter 3

3. Density matrix and Optical Bloch Equation (OBE)

3.1. Density matrix

3.1.1. Pure and mixed states

A quantum system defined in [43] with state vector denoted by $|\psi\rangle$ can be described with orthonormal basis states $|u_n\rangle$ from superposition of the quantum eigenstates as followings;

$$|\psi\rangle = \sum_n C_n |u_n\rangle \tag{3.1}$$

The state $|u_n\rangle$ shows a discrete orthonormal basis of pure state while the condition of normalization for C_n, must be satisfy.

$$\sum_n |C_n|^2 = 1 \tag{3.2}$$

If a quantum system has two or more subsystem that are entangled then each subsystem must be treated as a mixed as a mixed state even if the whole

system is in a pure state. The state of the system may be $|\psi_1\rangle$ with probability p_1 or $|\psi_n\rangle$ with probability p_n. This shows that:

$$p_1 + p_2 + \ldots + p_n = \sum_k p_k = 1 \tag{3.3}$$

A state vector can be described from the linear superposition of states.

$$|\psi\rangle = \sum_k C_k |\psi_k\rangle \tag{3.4}$$

3.1.2. Density operator in terms of density matrix

A density matrix is a matrix used to describe a quantum system in a mixed state. Preparing a two-level quantum system with upper excited level state $|a\rangle$ and lower ground state $|b\rangle$ as shown in Fig. 3.1, these two states are normalized as well as orthogonal to each other.

$$\langle a|a\rangle = \langle b|b\rangle = 1 \text{ (Normalization condition)}$$

$$\langle a|b\rangle = \langle b|a\rangle = 0 \text{ (Orthogonal condition)}$$

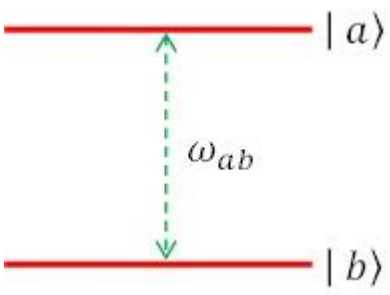

Fig. 3.1 A simple two-level system.

For this system a mixed state vector is defined as,

$$|\psi\rangle = C_a|a\rangle + C_b|b\rangle \tag{3.5}$$

C_a and C_b are the probability amplitudes. If A is any operator then the expected value is:

$$\langle A\rangle = \langle\psi|A|\psi\rangle = |C_a|^2 A_{aa} + |C_b|^2 A_{bb} + C_a^* C_b A_{ab} + C_b^* C_a A_{ba} \tag{3.6}$$

For multi-level system,

$$\langle A\rangle = \langle\psi|A|\psi\rangle = \sum_{nm} C_n^* C_m A_{nm} \tag{3.7}$$

Then the expected value of state vector in the orthonormal basis $\{|u_m\rangle\}$ can be written as,

$$\langle u_m|\psi\rangle\langle\psi|u_n\rangle = C_n^* C_m \tag{3.8}$$

$$|\psi\rangle\langle\psi| = \rho \tag{3.9}$$

$|\psi\rangle\langle\psi|$ is an operator which is a projector vector (only for pure state) and can be solved by dyadic product, where ρ is called the density operator and equation (3.8) can be written as

$$\langle u_m|\rho|u_n\rangle = \rho_{mn} = C_n^* C_m \tag{3.10}$$

3.1.3. Properties of density operator

Properties of a density operator in pure state and mixed state are presented in table 3.1.

	Pure state	Mixed state	Comments
a.	$\rho^{\dagger} = \rho$	$\rho^{\dagger} = \rho$	For Hermitian operator
b.	$Tr\rho = 1$	$Tr\rho = 1$	Sum of diagonal elements of ρ matrix =1
c.	$\langle A \rangle = Tr\{\rho A\} = Tr\{A\rho\}$	$\langle A \rangle = Tr\{\rho A\} = Tr\{A\rho\}$	Expected value
d.	$i\hbar \frac{d}{dt}\rho = [H, \rho]$	$i\hbar \frac{d}{dt}\rho = [H, \rho]$	Schrödinger equation in commutator form
e.	$\rho^2 = \rho$	$\rho^2 \neq \rho$	
f.	$Tr\rho^2 = 1$	$Tr\rho^2 \neq 1$ $Tr\rho^2 < 1$	For both states we can write $Tr\rho^2 \leq 1$

Table 3.1 Comparison of properties of density operator between pure and mixed states.

Density operator can define the population and coherence in the multi-level atomic system between the states. Equation (3.10) can be written as,

$$\rho_{nn} = \langle u_n | \rho | u_n \rangle \tag{3.11}$$

For mixed states,

$$\rho_{nn} = \sum_k p_k \langle u_n | \rho_k | u_n \rangle$$

From equation (3.9)

$$\rho_{nn} = \sum_k p_k \langle u_n | \psi_k \rangle \langle \psi_k | u_n \rangle$$

$$\rho_{nn} = \sum_k p_k |\langle u_n | \psi_k \rangle|^2 \tag{3.12}$$

From equation (3.12), it is concluded that the ρ_{nn} (diagonal terms) is called *populations* because ρ_{nn} is the probability of $|u_n\rangle$ in the state ρ. Similarly, equation (3.10) can be solved for ρ_{nm} then,

$$\rho_{nm} = \sum_k p_k \langle u_n | \rho_k | u_m \rangle = \sum_k p_k c_n^{(k)} c_n^{(k)*} \tag{3.13}$$

In equation (3.13), ρ_{nm} are the off-diagonal terms which shows the interference effect between $|u_n\rangle$ and $|u_m\rangle$. Therefore these terms are called "*coherences*".

3.2. Optical Bloch equations (OBE) for two-level system

Supposing a two level system with upper state as $|e\rangle$ with eigenvalue $\hbar\omega_e$ and lower state as $|g\rangle$ with eigenvalue $\hbar\omega_g$ as shown in Fig. 3.2, there is also a detuning δ in the laser light with optical frequency of ω_L which is linearly polarized along *x*-axis.

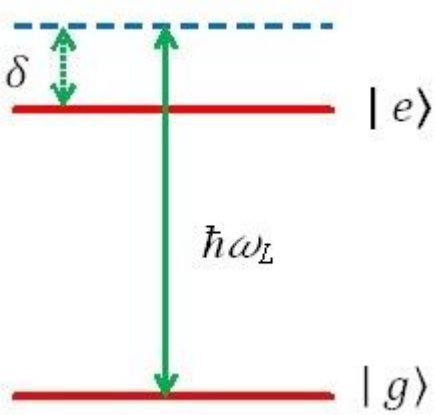

Fig. 3.2 A two-level system with laser beam of detuning δ

Then the total Hamiltonian (H) of the system is equal to the sum of Hamiltonian without light interaction (H_0) and the Hamiltonian with light interaction (H_1).

H_0 for two-levels can be define as,

$$H_0 = \hbar\omega_e |e\rangle\langle e| + \hbar\omega_g |g\rangle\langle g| \tag{3.14}$$

While in the interaction part (H_1), horizontally polarized light is interacting with the system. For horizontal polarization

$$H_1 = -exE$$

$$H_1 = -e\left(|e\rangle\langle g| x_{eg} + |g\rangle\langle e| x_{ge}\right)E$$

$$H_1 = -\left(|e\rangle\langle g| + |g\rangle\langle e|\right)d_x E \tag{3.15}$$

Note that x_{ee} and x_{gg} are equal to zero because there is no displacement from $|e\rangle$ to $|e\rangle$ or $|g\rangle$ to $|g\rangle$. And d_x is atomic dipole moment.

At this point we introduce equation for light and also an equation for Rabi frequency,

$$E = \frac{1}{2}\left(e^{-i\omega_L t} + e^{i\omega_L t}\right)E_0 \tag{3.16}$$

$$\Omega = \frac{d_x E_0}{\hbar} \tag{3.17}$$

After solving equations (3.15), (3.16) and (3.17) we get,

$$H_1 = -\frac{\hbar\Omega}{2}\left(|e\rangle\langle g| + |g\rangle\langle e|\right)\left(e^{-i\omega_L t} + e^{i\omega_L t}\right) \tag{3.18}$$

At this stage we consider Heisenberg picture of atoms, because the operators, observables dependent on time, but the state vector are time-independent.

In this case the operators for atoms movement between $|e\rangle$ and $|g\rangle$ are given as,

$\xi_+ = |e\rangle\langle g|$ and $\xi_- = |g\rangle\langle e|$ are varying in time $e^{i\omega_{eg}t}$ and $e^{-i\omega_{eg}t}$ as per Heisenberg picture respectively,

Therefore,

$$|e\rangle\langle g|e^{-i\omega_L t} = \xi_+ e^{-i\omega_L t} = e^{-i\omega_{ab}t}e^{-i\omega_L t} = e^{i(\omega_{eg}-\omega_L)t}$$

$$|e\rangle\langle g|e^{i\omega_L t} = \xi_+ e^{i\omega_L t} = e^{i\omega_{ab}t}e^{i\omega_L t} = e^{i(\omega_{eg}+\omega_L)t}$$

$$|g\rangle\langle e|e^{-i\omega_L t} = \xi_- e^{-i\omega_L t} = e^{-i\omega_{ab}t}e^{-i\omega_L t} = e^{-i(\omega_{eg}+\omega_L)t}$$

$$|g\rangle\langle e|e^{i\omega_L t} = \xi_- e^{i\omega_L t} = e^{-i\omega_{ab}t}e^{i\omega_L t} = e^{-i(\omega_{eg}-\omega_L)t} \quad (3.19)$$

Equations in (3.19) we are applying the rotating wave approximation (RWA) according to which the terms which oscillate rapidly are neglected. Terms in the equation (3.19) which oscillate with frequency $(\omega_{eg}+\omega_L)$ are neglected. From solving equation (3.18) and (3.19) we get,

$$H_1 = -\frac{\hbar\Omega}{2}\left(\xi_+ e^{-i\omega_L t} + \xi_- e^{i\omega_L t}\right)H \quad (3.20)$$

The density operator is governed by Schrödinger equation then,

$$\frac{d}{dt}\rho = \frac{1}{i\hbar}[H,\rho]$$

And also we are adding the decay term Γ in the equations then,

$$\dot{\sigma}_{ee} = -\Gamma\sigma_{ee} + i\frac{\Omega}{2}\left(\sigma_{eg}-\sigma_{ge}\right)$$

$$\dot{\sigma}_{gg} = \Gamma\sigma_{ee} - i\frac{\Omega}{2}\left(\sigma_{eg}-\sigma_{ge}\right)$$

$$\dot{\sigma}_{ge} = -i\delta\sigma_{ge} - i\frac{\Omega}{2}\left(\sigma_{ee}-\sigma_{gg}\right) - \frac{\Gamma}{2}\sigma_{ge}$$

$$\dot{\sigma}_{eg} = i\delta\sigma_{ge} + i\frac{\Omega}{2}\left(\sigma_{ee}-\sigma_{gg}\right) - \frac{\Gamma}{2}\sigma_{eg} \quad (3.21)$$

The equations in (3.21) are the optical Bloch equations for two-level systems. Thus we have $\sigma_{eg}e^{-i\omega_L t}=\rho_{eg}, \sigma_{ge}e^{i\omega_L t}=\rho_{ge}, \sigma_{ee}=\rho_{ee}$ and $\sigma_{gg}=\rho_{gg}$.

3.3. OBEs for Zeeman degenerate two-level system

In our case we are using ground hyperfine $5S_{1/2}$ to excited hyperfine $5P_{3/2}$ which is D_2 line at 780 nm for the transition of $F_g=3\rightarrow F_e=4$ ^{85}Rb atoms with degenerate magnetic sublevels as shown in Fig. 3.6.

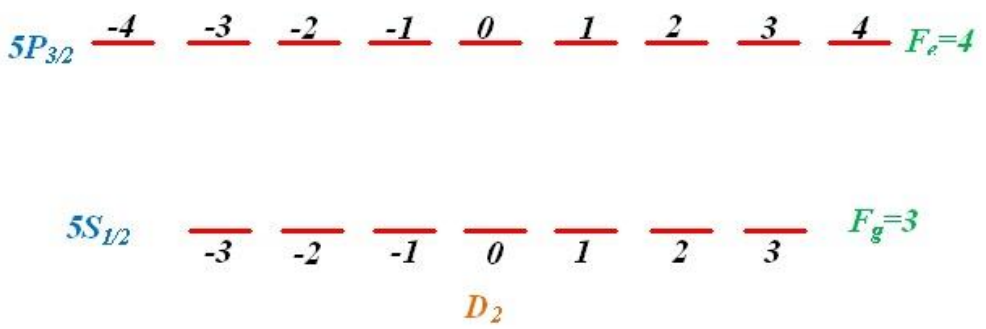

Fig. 3.3 Zeeman degenerate two-level system for the transition $F_g=3\rightarrow F_e=4$ in ^{85}Rb.

It is clear from the Fig. 3.6 that there is splitting due to Zeeman effect, therefore, the magnetic potential energy can be added into the atomic Hamiltonian.

$$H_A=\sum_{m=-4}^{4}\left(\hbar\omega_0+\mu_B g_e B m_e\right)|e_m\rangle\langle e_m|+\sum_{m=-3}^{3}\mu_B g_g B m_g\,|g_m\rangle\langle g_m| \quad (3.34)$$

where, $\mu_B g_e B m_e$ and $\mu_B g_g B m_g$ are the magnetic potential energy of the sublevels in excited and ground state, respectively.

The interaction part of the Hamiltonian is defined as,

$$V = \frac{1}{2}\hbar\Omega_1 \sum_{q=-1}^{1}\sum_{m=-3}^{3} c_q C_{F_g=3,m}^{F_e=4,m+q} \left|e_{m+q}\right\rangle\left\langle g_m\right| e^{-i\omega_1 t} + c.c \tag{3.35}$$

In equation (3.35) q values are determine by Table 2.1. Now, the spontaneous decay for multilevel can be defined as,

$$\left\langle e_m \left| (\dot{\rho})_{sp} \right| e_{m'} \right\rangle = -\Gamma \left\langle e_m \left| \rho \right| e_{m'} \right\rangle$$

$$\left\langle e_m \left| (\dot{\rho})_{sp} \right| g_{m'} \right\rangle = -\frac{\Gamma}{2} \left\langle e_m \left| \rho \right| g_{m'} \right\rangle$$

$$\left\langle g_m \left| (\dot{\rho})_{sp} \right| e_{m'} \right\rangle = -\frac{\Gamma}{2} \left\langle g_m \left| \rho \right| e_{m'} \right\rangle$$

$$\left\langle g_m \left| (\dot{\rho})_{sp} \right| g_{m'} \right\rangle = \Gamma \sum_{q=-1}^{1} C_{F_g=3,m}^{F_e=4,m+q} C_{F_g=3,m'}^{F_e=4,m'+q} \left\langle g_m \left| \rho \right| g_{m'} \right\rangle$$

(3.36)

Chapter 4

4. An ECDL laser system

4.1. Introduction

Stable and narrow linewidth laser system for high resolution spectroscopy has been used. Such laser can be bought from company or can be constructed in the lab. In our case we constructed semiconductor diode lasers with external cavity [36]. In this chapter we characterize ECDL for obtaining EIA line profile.

4.2. External cavity diode laser (ECDL)

4.2.1. Laser diode

In laser diode, light is produced by applying the current to the diode's active region which is in between the cladding layers (p and n type) as shown in Fig. 4.1 [36]. Therefore, the electron-hole pair is produced, which recombine and emit photons. The wavelength of laser light can be determined by the bandgap of the semiconductor material.

But unfortunately, there is a drawback that the light coming out of laser diode is diverging in an oval shape pattern. Such wide diverging beam is useless in any spectroscopic experiment. Therefore, this beam should be collimated so that all the output goes in one direction. This can be done by using a single lens; the focal point of a lens is also the point through which

all light parallel to its normal axis will converge. Hence, if we place our diode laser at the focal point of our collimating lens, all light from the diode laser that passes through the lens will exit parallel to the normal axis and all light that enters the face of the lens at normal incidence will be focused the diode laser as shown in Fig. 4.2.

In our laboratory, we used Thorlabs L785P090 laser diode with the aspheric collimating lens; Thorlabs C230TM-B lens. The collimating lens has a design wavelength of 780 nm and is AR coated for 600 nm to 1050 nm wavelength.

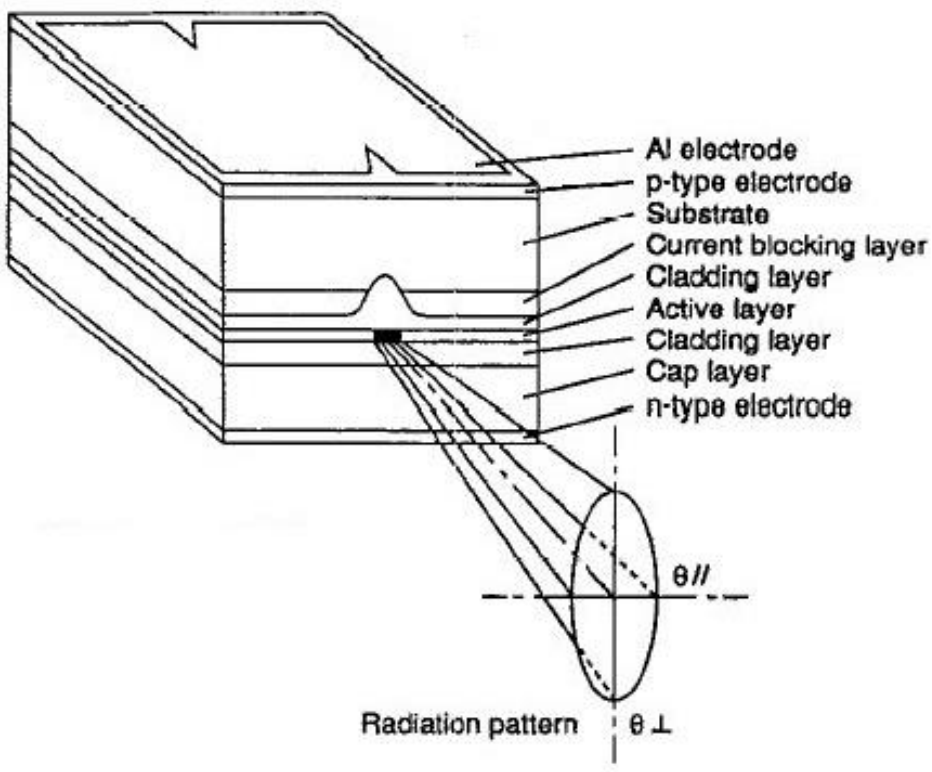

Fig. 4.1 A typical example of laser diode emitting light. [36]

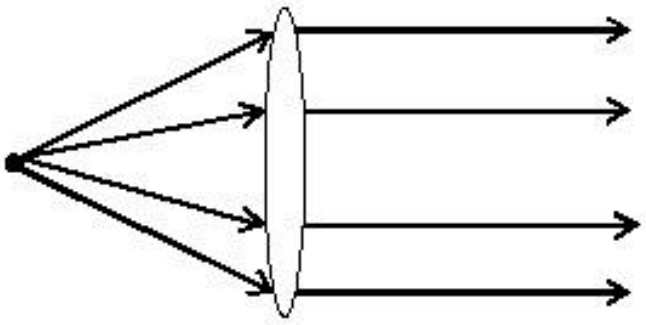

Fig. 4.2 Light from the surface of laser diode which is on the focus of collimated lens. After the collimating lens, laser rays get parallel.

4.2.2. The external cavity

ECDL is a tunable diode laser system with narrow bandwidth of less than one MHz and is very economical as compare to the commercial laser or dye lasers. In ECDL there is an external cavity which plays an important role. There is special Littrow angle, where first diffracted beam can reflect back from a holographic diffraction grating and form an external cavity (distance between laser diode and grating). The stationary condition for such laser is that an integer number of half wavelengths exactly match the resonant cavity length.

The diode is coupled to an external cavity that incorporates a diffraction grating as a wavelength-selective element, which then provides frequency-selective optical feedback to the diode laser via its output facet. The holographic diffraction grating is used in Littrow configuration [37-39] shown in Fig. 4.3.

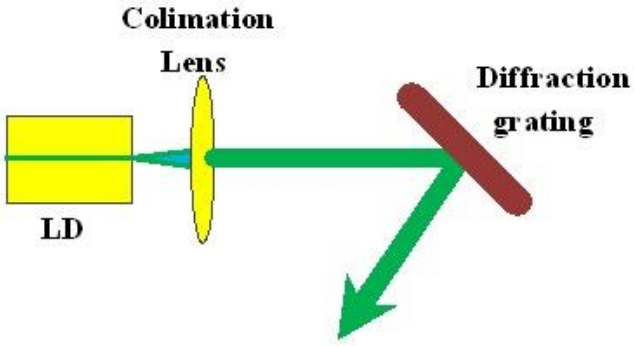

Fig. 4.3 External cavity diode laser output with Littrow configuration.

In Littrow configuration, the first order diffracted light that comes off the grating is sent directly back into the diode itself while the 0^{th} order can be used for the experiment. The grating act as wavelength selective mirror since it only reflects the light back that satisfies the diffraction equation

$$2d\sin\theta = m\lambda\,, \tag{4.1}$$

where d is the spacing between the lines, θ is the incident angle, m is the order (in our case m = 1) and λ is the wavelength of laser light.

In our lab we are using Edmunds optics holographic grating with part number 43775. Its dimensions are 12.7 mm x 12.7 mm with 1800 grooves per mm. For the fine tuning we can move the grating with the help of piezo-electronic transducer (PZT) which is located on the back of grating mount.

4.2.3. Temperature sensitivity

In ECDL, wavelength of laser light depends upon the length of the cavity. And interestingly, length of cavity changes with in temperature. The laser wavelength increased continuously by 0.3 nm/K, discontinuously pumping longitudinal modes approximately once per degree. This is called ‘mode

hopping'. For the stabilization of temperature in our case, we use thermoelectric cooler (TEC) of Thorlabs model TEC 3-6, which is placed in between the bottom of the base plate and a heat sink. And for further stabilization of temperature, laser system enclosed in Aluminum housing. Furthermore, laser system temperature is observed with the thermistor placed in the laser diode mount. We used Thorlabs TH10K thermistor in our ECDL.

4.3. Configuration of ECDL

For experiments of ultra-narrow EIA, we build an ECDL for both probe and pump beam. The output power of ECDL is 40 mW with wavelength of 780 nm. The temperature of ECDL is maintained at 21^{o}C with the help of PZT and thermistor placed in the base plate. The current and temperature of ECDL is maintained by Thorlabs ITC4001 Benchtop laser diode/TEC controller. The threshold current for the laser diode in our case is 30 mA and maximum value of current goes to 130 mA. But usually all the experimental data was collect in the range of 90 mA to 115 mA.

We have to align the grating and laser diode correctly. To do so, we have two alignments; horizontal and vertical alignment. There are two beams (zeroth order and first order) on the white screen out from the grating. In vertical alignment there are three screws on the base plate with which we can line up the two beams on same height and then after doing this we lock it by the center screw on the base plate. After completing vertical alignment, then we move to horizontal alignment which is very sensitive. A PZT is placed in between the horizontal alignment screw and the rare side of the grating. With this screw, we overlap the two beams exactly over a far distance (around 2 meters). Then with the help of CCD camera we do fine adjustment in which we observe the fluorescence due to two spots maximize. On next step we

reduce the current which results in decrease in fluorescence but by repeating the horizontal alignment we again increase the fluorescence. We repeat this process till the current goes to 27 mA.

We also study the typical characteristics of ECDL which plays an important role in our experiment i.e., injection current versus optical power as shown in Fig. 4.4.

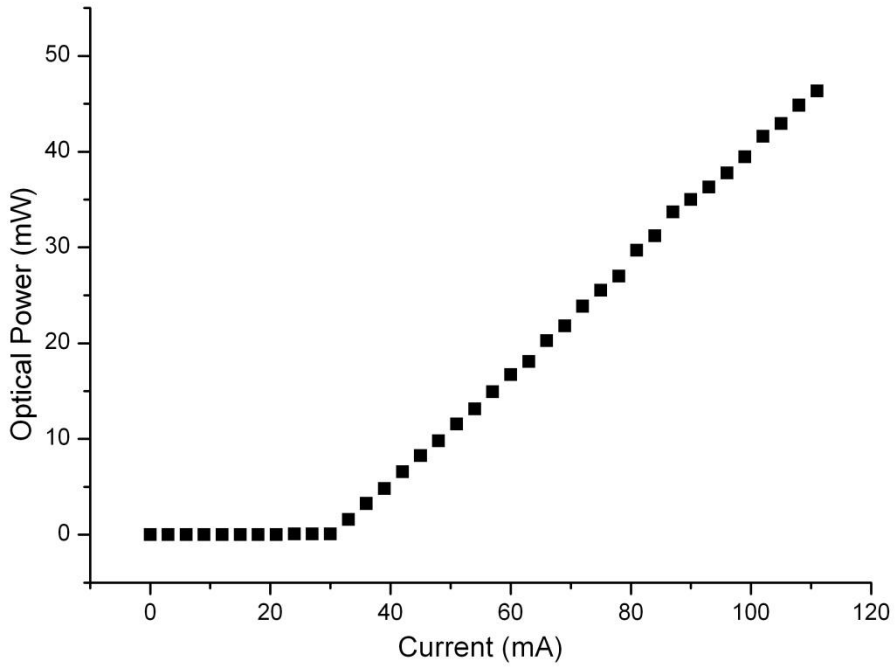

Fig. 4.4 A graph for injection current and optical power. It is clear that after ~30 mA which is the threshold value the relation between current and optical power is linear.

Fig. 4.4 represents the relationship between the injection current (on *x*-axis) to the laser diode and the optical power (on *y*-axis) of the ECDL. Observations are taken from 0 mA to 111 mA with the difference of 3 mA of current between the two observations. At the start, before 33 mA no optical power of laser beam was observed but after 33 mA which would be our

threshold value of injection current we observed a linear relationship between the two variables.

Chapter 5

5. EIA theory and experiment

5.1. Introduction

In quantum optics, we have two types of interference; 1) destructive interference, 2) constructive interference both have exactly opposite properties to each other. The destructive interference leads us to EIT, whereas EIA results from the constructive interference. This supports the previous statement that EIA is the opposite phenomenon of EIT.

EIA was first observed experimentally in 1998 by A.M. Akulshin *et al.* [12], then afterward in 1999 theoretical explanation of physical origins of EIA was given by A. V. Taichenachev *et al.* [11, 29] by using a simple analytically tractable model of a four-level *N*-configuration system.

In this chapter, I discussed theoretical calculations of EIA used by our group Hafeez *et al.* [32] to explain the phenomenon.

5.2. Theoretical treatment of EIA

In the theoretical explanation of EIA, we consider the transition from $F_g = 3 \rightarrow F_e = 4$ for ^{85}Rb atom D_2 line.

Consider we have two laser beams probe beam and pump beam with frequency of ω_{probe} and ω_{pump} with Rabi frequencies of Ω_1 and Ω_2

respectively. The system is ready by the pump beams and probe beam is observed for EIA phenomenon.

In the rest frame of an atom moving at velocity $\vec{v}$ the frequencies of probe and pump beam experienced by the atom are ω_1 and ω_2 given as;

$$\omega_1 = \omega_{probe} - k\nu$$

$$\omega_2 = \omega_{pump} - k\nu \tag{5.1}$$

Here $k = \left(2\pi/\lambda\right)$. Note that both the probe and pump beams are in the same direction in the rubidium cell i.e., co-propagating direction.

If ω_0 is the resonance frequency of the levels, then here we define the detunings of probe and pump beams as d_{probe} and d_{pump}.

$$d_{probe} = \omega_{probe} - \omega_0$$

$$d_{pump} = \omega_{pump} - \omega_0 \tag{5.2}$$

And also the detunings in the system are;

$$\delta_2 = \omega_2 - \omega_0$$

$$\delta_p = \omega_1 - \omega_2 \tag{5.3}$$

Equation (5.3) can be written as

$$\delta_2 = d_{pump} - k\nu$$

$$\delta_p = d_{probe} - d_{pump} \tag{5.4}$$

At this stage, we are defining our system for the transition from $F_g = 3 \rightarrow F_e = 4$ for 85Rb atom D_2 line in Fig. 5.1 and 5.2. The two Figs. show the two combination of polarization of probe and pump beams. $\left(\sigma^+ - \sigma^+, \sigma^+ - \sigma^-\right)$. Each combination has different interacting part of Hamiltonian of the system because of polarization.

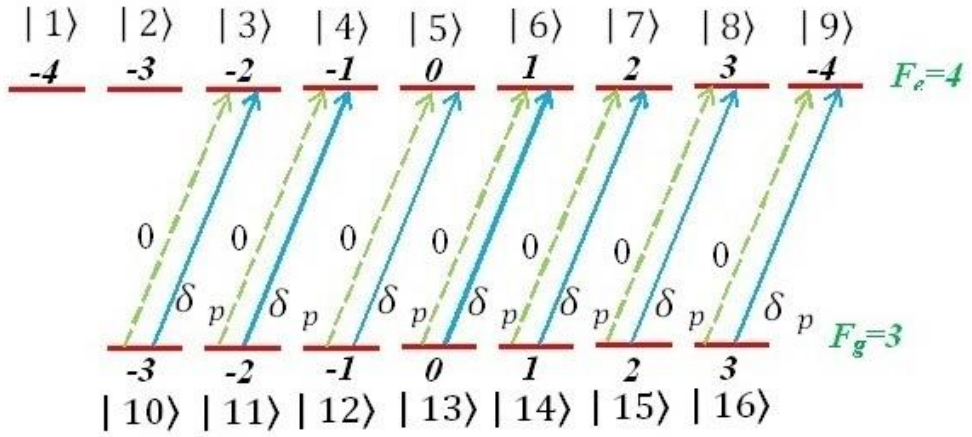

Fig. 5.1 ^{85}Rb atom transition from $F_g = 3 \rightarrow F_e = 4$. Probe (solid line) and pump (dotted line) beams both are right circularly polarized.

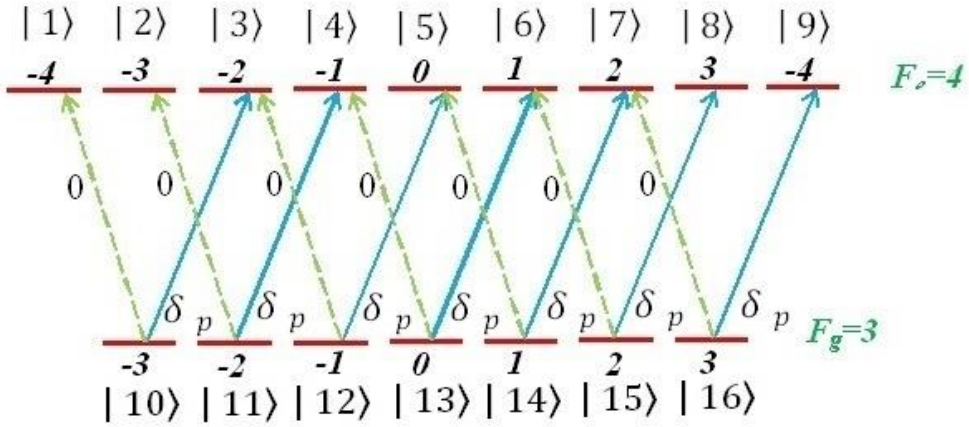

Fig. 5.2 ^{85}Rb atom transition from $F_g = 3 \rightarrow F_e = 4$. Probe (solid line) beam right circular polarization and pump (dotted line) beam left circular polarization.

The density matrix equation for the system is defined as,

$$\dot{\rho} = -\frac{i}{\hbar}\left[H_0 + H_1, \rho\right] + \dot{\rho}_{sp} \tag{5.5}$$

Here, H_0 is the Hamiltonian of excited state and is defined as;

$$H_0 = -\hbar\sum_{i=1}^{9}\left(\omega_2 - \omega_0\right)|i\rangle\langle i| \tag{5.6}$$

And $\dot{\rho}_{sp}$ is refer to spontaneous emission and is set as $\Gamma/2$ with Γ as a decay rate term of excited state. The interacting part is different for two cases because of the polarization of pump beam.

$$H_1 = \frac{\hbar}{2}\sum_{i=0}^{6}\left\{C_{10+i}^{3+i}\Omega_1 e^{-i\delta_p t}\left|3+i\right\rangle\left\langle 10+i\right| + C_{10+i}^{3+i}a_+\Omega_2\left|3+i\right\rangle\left\langle 10+i\right|\right\} + c.c. \tag{5.7}$$

The above equation is for the case of right circular polarization of both probe and pump beam as shown in Fig. 5.1. Here C is the Clebsch-Gordan coefficient for the transition (Fig. 2.4) and a_+ is refer as the coefficient of the right circular polarization of pump beam and is defined as.

$$a_+ = -\frac{1}{2}\left(1+\sin 2\varepsilon\right) - \frac{i}{2}\cos 2\varepsilon \tag{5.8}$$

In this case $\varepsilon = \pi/4$.

And if the two beams have opposite polarization i.e., pump beam has left circular polarization then, the interacting Hamiltonian part is,

$$H_1 = \frac{\hbar}{2}\sum_{i=0}^{6}\left\{C_{10+i}^{3+i}\Omega_1 e^{-i\delta_p t}\left|3+i\right\rangle\left\langle 10+i\right| + C_{10+i}^{1+i}a\_\Omega_2\left|1+i\right\rangle\left\langle 10+i\right|\right\} + c.c. \tag{5.9}$$

The coefficient for the left circular polarization of pump beam is defined as,

$$a\_ = \frac{1}{2}\left(1-\sin 2\varepsilon\right) + \frac{i}{2}\cos 2\varepsilon \tag{5.10}$$

And in this case $\varepsilon = -\pi/4$.

The population of each state is defining by density matrix diagonal element with the help of oscillation frequencies of $0, -\delta_p,$ and δ_p.

$$\rho_{jj} = \rho_{jj}^{(1)} + \left(\rho_{jj}^{(2)} + i\rho_{jj}^{(3)}\right)e^{-i\delta_p t} + \left(\rho_{jj}^{(2)} - i\rho_{jj}^{(3)}\right)e^{i\delta_p t} \qquad (5.11)$$

where $j = 1, 2\cdots, 16 =$ number of states of excited and ground state.

The off-diagonal term of density matrix which represents the coherence can be written as,

$$\rho_{3+j,10+j} = \rho_{3+j,10+j}^{(1)} + \rho_{3+j,10+j}^{(2)}e^{-i\delta_p t} + \rho_{3+j,10+j}^{(3)}e^{-i2\delta_p t} + \rho_{3+j,10+j}^{(4)}e^{i\delta_p t}$$

(5.12)

After solving equations from (5.5) to (5.12), we get differential equations similar to equation (3.31). Then from these differential equations we can find the absorption coefficient (α) which is the imaginary part of the susceptibility (χ). And can be define as,

$$\chi = \chi' + i\chi''$$

$$\alpha = \frac{\omega}{c}\chi''$$

In our case, α can be found by solving the differential equations of the density matrix elements.

$$\alpha_0\left(\delta_2, \delta_p, t\right) = -N_{at}\frac{3\lambda^2\Gamma}{2\pi\Omega_1}\sum_{j=0}^{6}\mathrm{Im}\left[C_{10+j}^{3+j}\rho_{3+j,10+j}^{(2)}\right], \qquad (5.13)$$

where N_{at} is the atomic number density of rubidium vapor cell. The absorption coefficient is then averaged over velocity distribution (transverse and longitudinal), then

$$\alpha = \frac{1}{t_{av}} \int_{0}^{t_{av}} dt \int_{-\infty}^{\infty} dv \frac{e^{-(v/u)^2}}{\sqrt{\pi} u} \alpha_0 \left(d_c - kv, d_p - d_c, t \right) \tag{5.14}$$

Chapter 6

6. The ultra-narrow EIA

Hafeez *et al.* [32] performed an experiment for the transition $F_g = 3 \rightarrow F_e = 4$ of ^{85}Rb D_2 line for thermal atoms. Experiment performed for same and orthogonal circular polarization $\left(\sigma^+ - \sigma^+, \sigma^+ - \sigma^-\right)$. The major difference between this experiment and previously performed EIA experiment was that the new approach of theoretical calculation of the spectrum are due to the transfer of Zeeman coherences in the magnetic sublevels of excited state $\left(\text{Thus } F_e = 4\right)$ In this experiment we used two separate ECDL for the probe and pump beam and it was the main reason that we were not able to observe the ultra-narrow EIA experimentally.

Therefore, for observing the ultra-narrow EIA experimentally we also used a single ECDL for both probe and pump beam. But the pump beam undergoes double-pass through two Acousto Optical Modulators (AOM), therefore, the pump beam can be scanned.

6.1. Theoretical background

We are considering the transition $F_g = 3 \rightarrow F_e = 4$ of ^{85}Rb D_2 line for thermal atoms. The energy band diagram can be shown in Fig. 6.1.

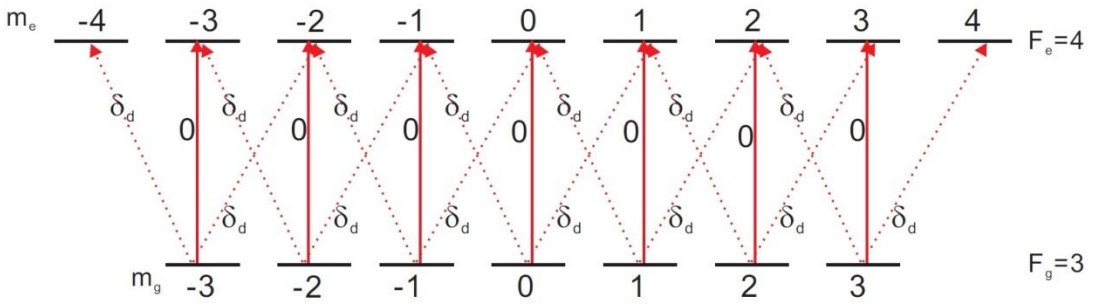

Fig 6.1 Energy level diagram for the $F_g = 3 \rightarrow F_e = 4$ transition of ^{85}Rb D_2 line. In which 0 and δ_d represent the off-set frequencies of pump and probe beam. [46]

The above Fig. 6.1 represents the polarization of probe and pump beam the transition. The pump beam (coupling) has linear polarization represent by the solid line while the probe beam have circular (left/right two case) polarization.

Consider we have two laser beams from one ECDL as probe beam and pump beam with Rabi frequencies of Ω_1 and Ω_2, respectively and both the beams are travelling in the same direction through the rubidium cell i.e., co-propagating direction. The system is ready by the pump beams and probe beam is observed for EIA phenomenon.

In the rest frame of an atom moving at velocity $\vec{v}$ the frequencies of probe and pump beam experienced by the atom are ω_1 and ω_2 given as;

$$\omega_1 = \omega_p - k\nu$$

$$\omega_2 = \omega_c - k\nu \qquad (6.1)$$

Here $k = \left(2\pi/\lambda\right)$. Note that

If ω_0 is the resonance frequency of the levels, then here we define the detunings of probe and pump beams as d_p and d_c.

$$d_p = \omega_p - \omega_0$$

$$d_c = \omega_c - \omega_0 \tag{6.2}$$

And also the detunings in the system are;

$$\delta_2 = \omega_2 - \omega_0 = d_c - k\nu$$

$$\delta_d = \omega_1 - \omega_2 = d_p - d_c \tag{6.3}$$

The density matrix equation under rotating wave approximation for the system is define as,

$$\dot{\rho} = -\frac{i}{\hbar}[H, \rho] + \dot{\rho}_{sp} = -\frac{i}{\hbar}[H_0 + H_1, \rho] + \dot{\rho}_{sp} \tag{6.4}$$

where H is the total Hamiltonian of the system and is defined as the sum of Hamiltonian of unperturbed atoms and Hamiltonian of atoms with interaction of light.

The Hamiltonian of unperturbed atom is similar to the chapter 5 equation (5.6.a) and (5.6.b) which is only for the excited state and we can rewrite as,

$$H_0 = -\hbar \begin{bmatrix} \delta_2 & 0 & 0 & 0 & 0 & 0 & 0 & 0 & 0 \\ 0 & \delta_2 & 0 & 0 & 0 & 0 & 0 & 0 & 0 \\ 0 & 0 & \delta_2 & 0 & 0 & 0 & 0 & 0 & 0 \\ 0 & 0 & 0 & \delta_2 & 0 & 0 & 0 & 0 & 0 \\ 0 & 0 & 0 & 0 & \delta_2 & 0 & 0 & 0 & 0 \\ 0 & 0 & 0 & 0 & 0 & \delta_2 & 0 & 0 & 0 \\ 0 & 0 & 0 & 0 & 0 & 0 & \delta_2 & 0 & 0 \\ 0 & 0 & 0 & 0 & 0 & 0 & 0 & \delta_2 & 0 \\ 0 & 0 & 0 & 0 & 0 & 0 & 0 & 0 & \delta_2 \end{bmatrix} \tag{6.5}$$

And the second part of the Hamiltonian which represents the interaction with light can be defined as,

$$H_1 = \underbrace{\frac{\hbar}{2}\sum_{q=\pm1} a_q \sum_{m=-3}^{3} C_{3,m}^{4,m+q}\Omega_1 \left|F_e, m+q\right\rangle\left\langle F_g, m\right|}_{probe} + \underbrace{\frac{\hbar}{2}\sum_{m=-3}^{3} C_{3,m}^{4,m}\Omega_2 \left|F_e, m\right\rangle\left\langle F_g, m\right|}_{pump} \tag{6.6}$$

where $a_{\pm}$ is for the Hermitian conjugate. Also $C_{3,m}^{4,m+q}$ and $C_{3,m}^{4,m}$ represent the transitional strength for circular and linear polarization of light respectively.

Lastly, the spontaneous decay can be defined in the matrix form.

$$\dot{\rho}_{sp} = \left(\begin{array}{c|c} \overset{A}{-\Gamma \rho_{ij}} & \overset{B}{-\frac{\Gamma}{2}\rho_{ij}} \\ \hline \overset{C}{-\frac{\Gamma}{2}\rho_{ij}} & \overset{D}{7\times 7} \end{array} \right)$$

For the transition of $F_g = 3 \rightarrow F_e = 4$ ^{85}Rb, the $\dot{\rho}_{sp}$ can be represent by the 16x16 matrix. For further description we divide this matrix into four parts. Part A represents the decay of excited state. Part B and C represent the coherence term between the excited and ground state. And part D represents the decay of the ground state. In our case we ignore part D because we do not consider buffer case in our rubidium vapor cell.

Therefore, the spontaneous decay can written in equation form as,

$$\begin{aligned} \dot{\rho}_{sp} = & -\Gamma \sum_{m=-4}^{m=4} \sum_{m'=-4}^{m=4} |F_e, m\rangle\langle F_e, m'| \\ & -\frac{\Gamma}{2} \sum_{m_e=-4}^{4} \sum_{m_g=-3}^{3} \left(|F_e, m_e\rangle\langle F_g, m_g| + |F_g, m_g\rangle\langle F_e, m_e| \right) \\ & +\Gamma \sum_{m=-3}^{3} \sum_{m'=-3}^{3} \sum_{q=-1}^{1} C_{3,m}^{4,m+q} C_{3,m'}^{4,m'+q} |F_e, m+q\rangle\langle F_e, m'+q| \end{aligned} \qquad (6.7)$$

The last term in equation (6.7) cannot explain by the matrix form of spontaneous decay. Here last term shows that the decay from the excited state to the ground state is depend upon the transitional strength between the sublevels.

By solving equation from (6.4) to (6.6), the absorption coefficient found to be,

$$\alpha = -\frac{3\lambda^2}{2\pi}\frac{N_{at}}{\Omega_1}\int_0^{t_{av}}\frac{dt}{t_{av}}\int_{-\infty}^{\infty}\frac{dv}{\sqrt{\pi}u}e^{-(v/u)^2}\ \mathrm{Im}\left[\sum_{q=\pm1}\sum_{m=-3}^{3}a_q^* C_{3,m}^{4,m+q}\rho_{e_{m+q},g_m}^{(1)}\right]$$

where N_{at} is the atomic vapor density in the cell and t_{av} is the transit time for crossing the laser beam.

6.2. Experimental setup for Ultra-narrow EIA spectra

In our studies the ultra-narrow EIA spectra is studied with respect to power dependences as well as polarization dependences.

As discussed earlier, that for observing the ultra-narrow EIA we are using a single ECDL for both probe and pump beam. In such a way that pump beam can double-pass through the two AOMs so that scanning of pump should be possible. The experimental setup, used for the dependence of ultra-narrow EIA on power is shown in Fig. 6.2.

An ECDL of wavelength 780 nm was used for producing the pump and probe beams. The beam coming out from ECDL was vertically polarized laser beam, after passing through the optical insulator (OI), it first divided by window (W1) into probe (reflected) and pump (transmitted) beams. After window (W1), the reflected probe beam further divided equally into two beams by beam splitter (BS). The transmitted beam from the BS was used as a probe beam for ultra-narrow EIA experiment while the reflected beam used

for saturation absorption signals. With the help of SAS signals and lock-in amplifier probe beam locked on the transition $F_g = 3 \rightarrow F_e = 4$ of ^{85}Rb D_2 line. Onward, the probe beam for the ultra-narrow EIA experiment was expanded to the size of 3.5 mm with the help of beam expander (BE). The polarization probe laser beam was made perfectly vertical just before first common beam splitter (BS) using a half wave plate.

The scanning of pump laser frequency is achieved by using two acousto-optic modulators (AOM). The transmitted beam from window W1 (pump beam) which had vertical polarization with optical frequency of ω_0 fall on polarized beamsplitter (PBS) and then reflected 90^o. At this point, the vertically polarized pump beam passed through AOM1. AOM1 adjusted in such a way that the pump beam achieved Bragg's angle. With very sophisticated alignment of AOM1 we get zero and first order of the laser beam and in our experiment we only used 1st order, therefore, we blocked zeroth order of light. To change the polarization state of the first order up-shifted pump beam from vertical polarization, this beam passed through quarter wave plate and focused on mirror. The reflected beam traced back to the original path passing through all optics and then into AOM1. As the beam had passed through AOM1 twice which results the beam frequency up-shifted to $(\omega_0 + 2\omega_1)$, where ω_1 is the central frequency of AOM1.After the double-pass of pump beam from AOM1, the polarization of pump beam had changed from vertical to horizontal polarization because the beam also passed twice through quarter wave plate. Horizontally polarized pump beam can transmit through the PBS. And this up-shifted $(\omega_0 + 2\omega_1)$ pump beam was sent into AOM2 with central frequency ω_2 for double pass down shift in frequency (for down shifted frequency we took opposite of up shifted 1st

order) which results as $(\omega_0 + 2\omega_1 - 2\omega_2)$.

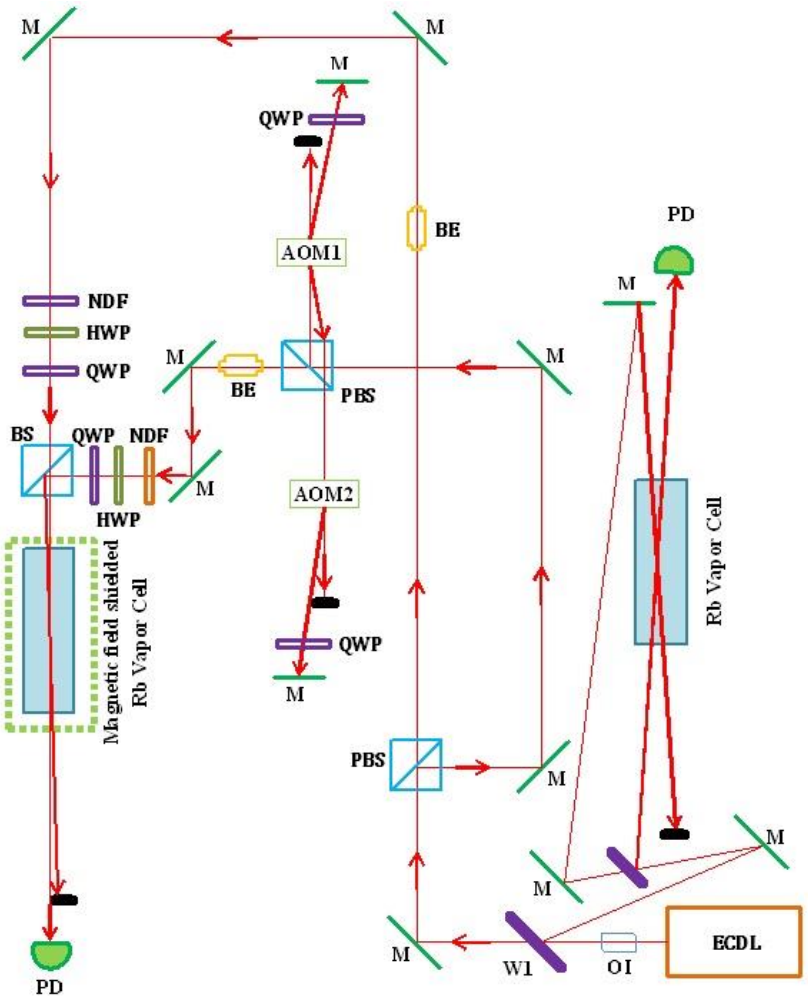

OI= Optical Insulator
BS= Beam Splitter
PBS= Polarize Beam Splitter
M= Mirror
QWP= Quarter Waveplate
HWP= Half Waveplate
AP= Aperture
NDF= Neutral Density filter
PD= Photo Diode
W= Window
BE= Beam Expander

Fig. 6.2 Experimental arrangement for observing ultra-narrow EIA by using single ECDL for probe and pump beam.

As shown in Fig. 6.2 the pump beam passed through quarter wave plate twice, therefore, the polarization of this beam changed from horizontal to vertical just before PBS. The pump beam then reflected by PBS. A separate beam expander was used to expand the pump lasers beam equal to 4mm in diameter. Similar to probe beam, the polarization of pump beam was made perfectly vertical before first common beam splitter (BS) by using a half wave plate.

The experimental arrangement can be used for different configurations of polarization of probe and pump lasers beams. For instance, the linear-parallel polarization configuration $(\pi\|\pi, \pi\perp\pi)$ or same-circular polarization $(\sigma^+-\sigma^+, \sigma^--\sigma^-)$ configuration have been used. In our setup, both probe and pump beams were vertically polarized and to make sure this polarization we were using half wave plates for both beams, which were double checked by using polarimeter. With these two half wave plates we can easily achieve both case of linear-parallel polarization. Furthermore, by the addition of two more quarter wave plates with optics axis angle $\varepsilon = 45$ with respect to y-axis were placed just before the BS which prepared the same-circular polarization configuration $(\sigma^+-\sigma^+, \sigma^--\sigma^-)$ of probe and pump lasers beams. Both beams mixed at BS and well overlapped in the vapor cell but at long distance these two beams separated apart. The pump beam was blocked while the probe beam focused on photodiode.

Likewise, this arrangement can also be used for case linear-perpendicular polarization configuration $(\pi\perp\pi)$ and circular-orthogonal polarization configuration $(\sigma^+-\sigma^-, \sigma^--\sigma^+)$ of probe and pump laser beams. For linear-perpendicular configuration removed the quarter wave plates before the common BS and change the optical axis of one half wave plate so that

polarization changed from vertical to horizontal. Therefore, one beam vertical polarized while the other was horizontally polarized. If we placed quarter wave plates on the path of probe and pump beams before the common BS then we can achieve the circular-orthogonal $\left(\sigma^{+}-\sigma^{-},\sigma^{-}-\sigma^{+}\right)$ configuration.

A ramping voltage of 125 V_{pp} (peak to peak) allows the pump beam to detune in the range of 5 MHz. The intensities of both beams were controlled by two separate neutral density filters (NDF). Maximum power of control beam which is used in this experiment was 1mW while the power of probe beam used here between 10 and 20 μW.

6.3. Power dependence of spectral features of ultra-narrow EIA

Power dependences of the same and orthogonal polarization cases of pump and probe lasers are described well in previous works. [32, 45, 46] Here we have summaries of works in the following cases.

Add new reference

Linear-parallel polarization $(\pi\|\pi)$ configuration

Linear-perpendicular polarization $(\pi \perp \pi)$ configuration

Circular-perpendicular polarization $(\sigma^{+} - \sigma^{-})$ configuration

6.3.1. Linear-parallel polarization $(\pi\|\pi)$ configuration

For observing the power dependences of EIA we first observe spectra for the case of linear- parallel polarization $(\pi\|\pi)$ case. Fig 6.3 shows the spectra of a given case in which vertical axis represents the probe absorption in arbitrary unit and horizontal axis show the pump detuning in MHz and the width of spectrum in Fig. 6.3 is 5 MHz. Above high power of pump beam at 800 μW, no EIA is observed and with the decrease power of pump beam the EIA peak gets noticeable. At 200 μ W the linewidth of the ultra-narrow EIA spectrum is ~270 kHz much narrower than the 6 MHz linewidth of upper state level.

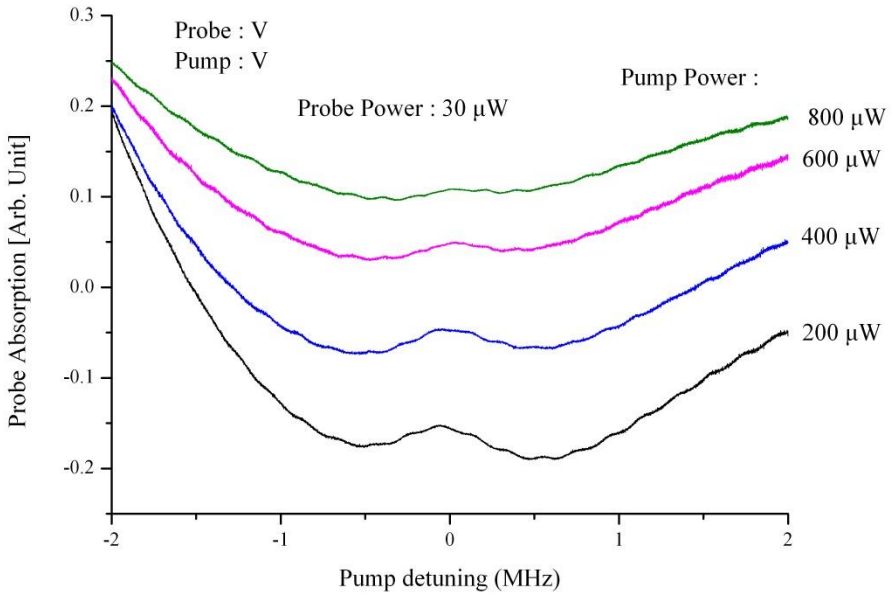

Fig. 6.3 Experimentally observed EIA power dependence spectra for the case of linear-parallel polarization configuration of probe and pump laser beams.

6.3.2. Linear-perpendicular polarization $(\pi \perp \pi)$ configuration

For the linear perpendicular polarization condition we arrange the experiment in which probe beam has horizontal polarization while pump beam has vertical polarization. Probe power is fixed at 30 μ W. In theoretical calculations the power of probe keep very small like less than 10 μ W but experimentally at such low power of probe beam no absorption peaks observed, and this is due to the laboratory environmental conditions. The experimental observation of EIA shows that with increase in power of pump beam which directly related to the Rabi frequency of the pump beam there is

an increase in the size of peak.

The spectra are not split into two parts with the increased power of pump beam because theoretically it is expected that the spectra split at high power. More pump power with Rabi frequency of pump laser (typically above 2 mW power) is required to observe those. Our present maximum power is around ~750 μW so that we could not observe those effects. For this experiment the beam size of both probe and pump beam is 4 mm.

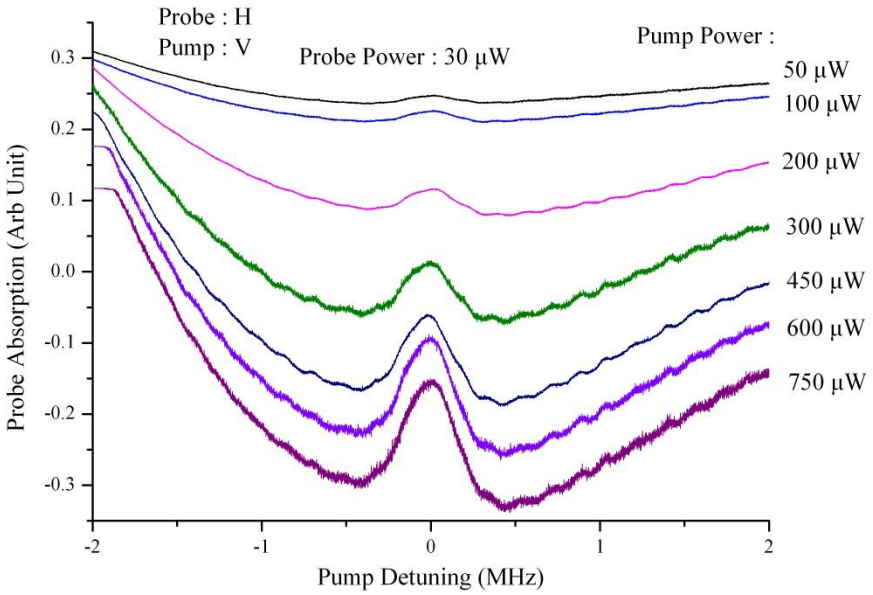

Fig. 6.4 EIA power dependence spectra in the case of linear-perpendicular polarization configuration of probe and pump beams with respect to the change of pump powers.

6.3.3. Orthogonal-circular polarization $\left(\sigma^{+}-\sigma^{-}\right)$ configuration

Polarization of probe beam has right circular and polarization of pump beam has left circular with probe beam power fixed at 30 μW while

observations were taken at different powers of pump beam. The beam size of each beam is 4 mm. The trend of increasing peak height with increasing power of pump beam is opposite to that in the case of linear-parallel polarization configuration.

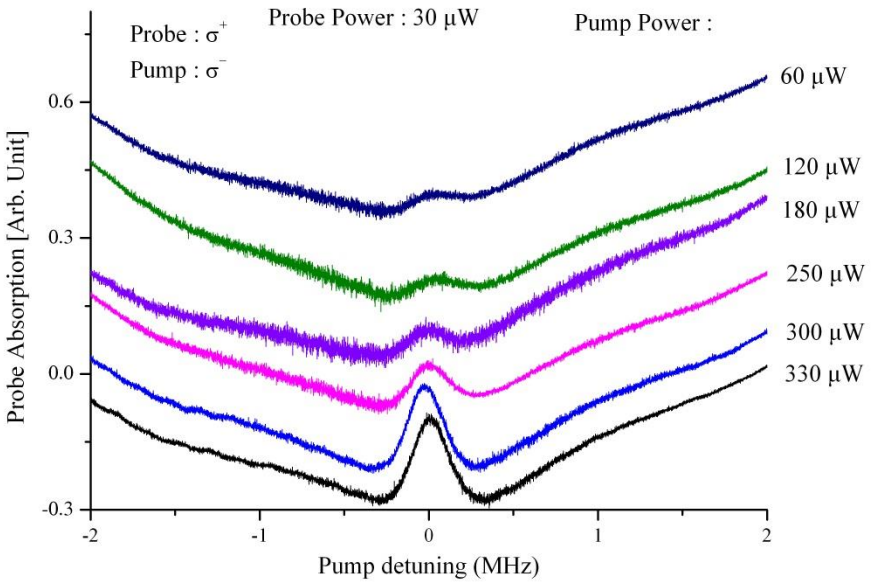

Fig. 6.5 EIA power dependence spectra in the case of circular-orthogonal polarization configuration of probe and pump beams with respect to the changes of pump powers.

6.4. Polarization dependence of spectral features of ultra-narrow EIA

In this section EIA spectra with respect to various polarizations of pump beams are studied in the following linear and circular cases of fixed polarizations of probe beams.

6.4.1. Linear polarization case

In linear polarization case, we remove the quarter wave plates before the common BS in Fig. 6.2. And with the help of half wave plates we make the eccentricity of probe and pump beam maximum i.e., $(\pi \perp \pi \rightarrow H - V)$. And every observation is taken by changing the optical axis of half wave plate by $\varepsilon = 15$ until polarization become parallel.

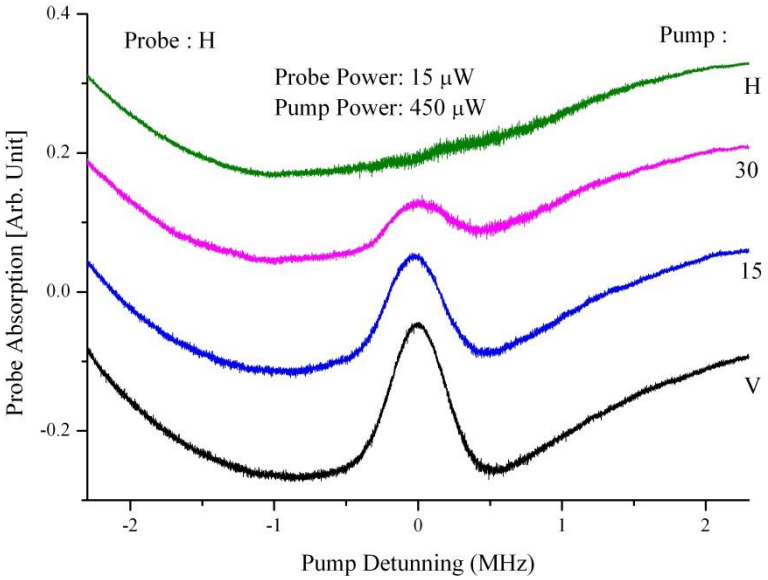

Fig. 6.6 EIA polarization dependence spectra in the case linear polarization of probe and pump beams with respect to the changes of pump polarization.

Fig. 6.7 shows the polarization dependence of EIA for the case of linear polarization configuration of probe and pump beam. As similar to all other observation, the *y*-axis has probe absorption with arbitrary units and also the *x*-axis has pump detuning in MHz from -2.5 MHz to 2.5 MHz which makes the spectrum of 5 MHz. And because of 5 MHz of spectrum we applied

125 V_{pp} ramping voltage to pump beam so that it detune from -2.5 MHz to 2.5 MHz. The beam size of each beam is 4mm before the common BS where the mixed. Power of each beam is fixed i.e., probe power fixed at 15 μ W and pump power at 450 μ W.

The probe beam is fixed and locked to transition between $F_g = 3 \rightarrow F_e = 4$ of thermal ^{85}Rb atoms while pump beam is scanning. From observation it is observed that the EIA peak is smaller when eccentricity between the beams is less. And when the eccentricity between the probe and pump beam maximum means when both beams have perpendicular polarization $(H - V)$. And it depends upon the transitional strength and optical pumping effect, these two parameters gets maximum effect on the EIA peak when polarization become perpendicular because both the beams were not sharing the same magnetic sublevels. The linewidth of EIA peak at vertical polarization of pump beam is ~300 kHz which is narrower than the 6 MHz.

6.4.2. Circular polarization case

For the case of circular polarization dependence on EIA spectra, we placed the two quarter wave plates in front of common BS in such a way that both the probe and pump beams are orthogonally polarized. And each observation is made by changing the eccentricity $\varepsilon = +15$ of pump beam and probe beam polarization is fixed on right circular polarization.

Fig. 6.8 shows the EIA spectra with respect to variations of polarizations of pump beam with fixed right circular polarization of the probe beam. The power of probe and pump beams are 15 μ W and 300 μ W, respectively. The

beam sizes of both beams are 4 mm.

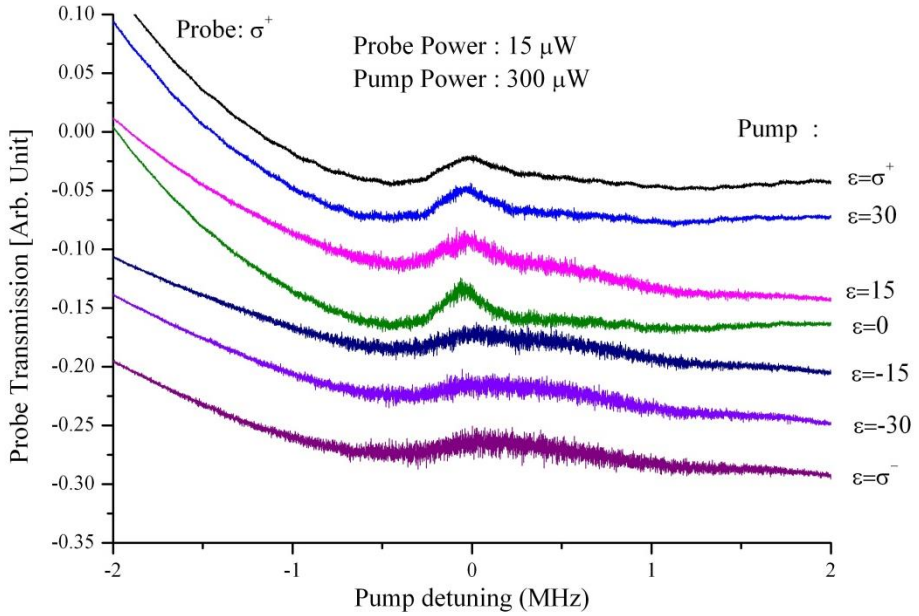

Fig. 6.7 EIA polarization dependent spectra in the case of right circular polarization of probe beam with respect to the changes of pump polarizations.

Our experimental spectra show a similar behavior like in theoretical calculation in Fig. 6.8. Although the two beams have same polarizations, an EIA spectrum is observed as shown in the theoretical calculation. Signal sizes increase as polarization of pump beam varies from same polarization (ε = +45) as the probe beam to linear polarization (ε = 0) of the pump beam as shown in the theoretical calculation. And EIA signal is maximum when the polarization of pump beam is linear (ε = 0). Signal sizes decrease as polarization of pump beam varies from linear polarization (ε = 0) of the pump beam to orthogonal polarization (ε = -45) as shown in the theoretical calculation. In theoretical observation EIA peak get split into two after ε =0 until both beams are orthogonally polarized. But in experimental observation the splittings are not resolved although line broadenings of the EIA signals,

which may be due to weak split features of the spectral lines.

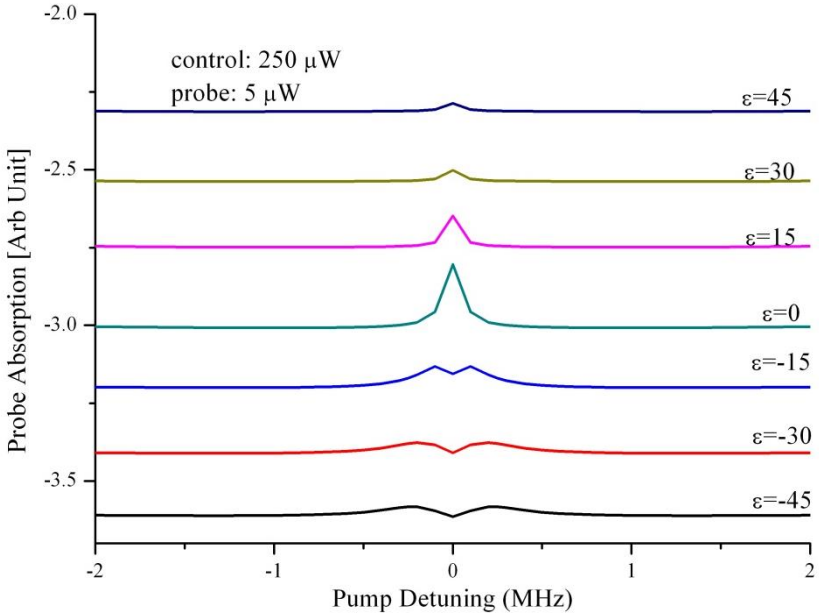

Fig. 6.8 Theoretical calculation of EIA spectra with respect to polarization dependence in the case of fixed circular polarization of probe and the changes of pump polarizations.

Fig. 6.8 shows the theoretical calculations for the ultra-narrow EIA when probe beam has right-circular polarization (ε = +45) and initial pump beam has left circular polarization (ε = -45), where the polarizations are varied. Both probe and pump beams have fixed power i.e., 5 μ W and 250 μ W. Each observation was done every the eccentricity of 15 till both beams achieved same polarization. The vertical axis represents the probe absorption with arbitrary units and the horizontal axis represents the pump detuning in MHz in the ranges from -2 MHz to 2 MHz (total of 4 MHz).

When the eccentricity between the pump and probe was 0, maximum EIA signal is obtained theoretically. Interesting features are split ultra-narrow EIA signals near $\varepsilon = -45$. When both pump and probe beams have same

polarization $\varepsilon = +45$, the smallest EIA signal is obtained as expected. According to theoretical calculation largest EIA signal is at the linear polarization case of the pump laser where the polarization is composed of both $\varepsilon = -45$ and $\varepsilon = +45$.

7. Conclusion and outlook

7.1. Conclusions

We performed experiments for the transition $F_g = 3 \rightarrow F_e = 4$ of ^{85}Rb in D_2 transition line $\left(5S_{1/2} \rightarrow 5P_{3/2}\right)$ for arbitrary power and polarization dependences. To escape phase noise between two independent pump and probe lasers, one homemade laser system combined with AOMs is used to get those results. In power dependence of ultra-narrow EIA, for the same polarization cases the absorption peak become smaller as power increases. When the eccentricity between the pump and probe was 0, maximum EIA signal is obtained theoretically and experimentally. Although both pump and probe beams have same polarization $\varepsilon = +45$, the smallest EIA signal is obtained as expected theoretically. According to theoretical calculation largest EIA signal is at the linear polarization case of the pump laser as EIA signal in the case of circular polarization in the experiment. These trends should be investigated in cold atom experiments in the future, which may different trends due to cold atom instead of thermal atom.

7.2. Outlook

Signal to noise ratio of the observed EIA spectral features should be enhanced to investigate physical origins of EIA signals depending on the variations of pump polarizations in the near future. After these clarifications, next step is to work on magneto optical trap (MOT) for rubidium atom and explore all the features of ultra-narrow EIA for cold atom experimentally. Our group is planning to produce a stable cycling MOT as well as non-

cycling MOT whose features are not clearly understood previously for both isotopes of rubidium atom.

References

1- S. Mitra, M.M. Hosain, B. Ray, P.N. Ghosh, S. Cartaleva, D. Slavov, "Online shape of electromagnetically induced transparency in a multilevel system," Opt. Comm. **283**, 1500 (2010).

2- S. M. Iftiquar, Vasant Natarajan, "Line narrowing of electromagnetically induced transparency in Rb with a longitudinal magnetic field," Phys. Rev. A **79**, 013808 (2009).

3- Ho-Jung Kim, Han Seb Moon, "Electromagnetically induced absorption with sub-kHz spectral width in a paraffin-coated Rb vapor cell," Opt. Exp. **19**, 168 (2010).

4- H. S. Moon, H R Noh, "Optical pumping effect in ladder-type electromagnetically induced transparency of $5S_{1/2}$-$5P_{3/2}$-$5D_{3/2}$ transition of ^{87}Rb," J. Phys. B **44**, 055004 (2011).

5- G. Alzetta, S. Cartaleva, Y. Dancheva, Ch. Andreeva, S. Gozzini, L. Botti, A Rossi, "Coherent effects on the Zeeman sublevels of hyperfine states at the D_1 and D_2 lines of Rb," J. Opt. B **3**, 181 (2001).

6- G. Alzetta, A. Gozzini, L. Moi and G. Orriols, "An experimental method for the observation of R. F. Transitions and laser beat resonance in oriented Na vapor," Nuovo Cimento B **36**, 5 (1976).

7- K.-J. Boller, A. Imamoğlu and S. E. Harris, "Observation of Electromagnetically induced transparency," Phys. Rev. Lett. **66**, 2593 (1991).

8- M. D. Lukin, P. R. Hemmer, M. O. Scully, "Resonant nonlinear optics in phase-coherent media," Adv. Atom. Mol. Opt. Phys. **42**, 347

(2000).

9- A. B. Matsko, O. Kocharovskaya, Y. Rostovtsev, G. R Welch, A. S. Zibrov, M. O. Scully, “Slow, ultraslow, stored and frozen light,” Adv. Atom. Mol. Opt. Phys. **46**, 191 (2001).

10- N. V. Vitanov, M. Fleischhaurer, B. W. Shore, K. Bergmann, “Coherent manipulation of atoms and molecules by sequential laser pulses,” Adv. Atom. Mol. Opt. Phys. **46**, 55 (2001).

11- A. V. Taichenachev, A. M. Tumaikin, and V. I. Yudin, “Electromagnetically induced absorption in a four-state system,” Phys. Rev. A **61**, 011802 (1999).

12- A. M. Akulshin, S. Barreiro, and A. Lezama, “Electromagnetically induced absorption and transparency due to resonant two-field excitation of quasidegenerate level in Rb vapor,” Phys. Rev. A. **57** 2996 (1998).

13- A. Lezama, S. Barreiro, and A. M. Akulshin, “Electromagnetically induced absorption,” Phys. rev. A **59**, 4732 (1999).

14- A. Lezama, S. Barreiro, A. Lipsich, and A. M. Akulshin, “Coherent two-field spectroscopy of degenerate two-level systems,” Phys. Rev. A **61**, 013801 (1999).

15- A. Lipsich, S. Barreiro, A. M. Akulshin, and A. Lezama, “Absorption spectra of driven degenerate two-level atomic systems,” Phys. Rev. A **61**, 053803 (2000).

16- S. K. Kim, C. H. Lee, K. Kim, and J. B. Kim, “Observation of electromagnetically induced absorption in an open atomic systems regardless of angular momentum,” Phys. Rev. A **68**, 063813 (2003).

17- H.S. Chou, and J. Evers, “Dressed-atom multiphoton analysis of anomalous electromagnetically induced absorption,” Phys. Rev. Lett.

104, 213602 (2010).

18- C. Goren, A. D. Wilson-Gordon, M. Rosenbluh, and H. Friedmann, "Electromagnetically induced absorption due to transfer of population in degenerate two-level systems," Phys. Rev. A **70**, 043814 (2004).

19- C. Goren, A. D. Wilson-Gordon, M. Rosenbluh, and H. Friedmann, "Electromagnetically induced absorption due to transfer of coherence and to transfer of population," Phys. Rev. A **67**, 033807 (2003).

20- T. Zigdon, A. D. Wilson-Gordon, and H. Friedmann, "Absorption spectra for strong pump and probe in atomic beam of cesium atoms," Phys. Rev. **80**, 033825 (2009).

21- G. Z. Zhang, M. Katsuragawa, K. Hakuta, R. I. Thompson, and B. P. Stoicheff, "Sum-frequency generation using strong-field coupling and induced transparency in atomic hydrogen," Phys. Rev. A **52**, 1584 (1995).

22- Bo Gao, "Effect of Zeeman degeneracy on the steady-state properties of an atom interacting with a near-resonant laser field: Analytical results," Phys. Rev. A **48**, 2443 (1993).

23- Bo Gao, "Effect of Zeeman degeneracy on the steady-state properties of an atom interacting with a near-resonant laser field: Probe spectra," Phys. Rev. A **49**, 3391 (1994).

24- Shigeru Nakayama, "Optical pumping effects in high resolution laser spectroscopy," Phys. Scripta. **T70**, 64 (1997).

25- M. Kwon, K. Kim, H. D. Park, and J. B. Kim, "Dependence of EIA spectra on mutual coherence between coupling and probe field in Cs atomic vapor," J. Korean Phys. Soc. **40**, 452 (2002).

26- A. M. Akulshin, A. Cimmino, A. I. Sidorov, P. Hannaford, and G. I.

Opat, “ Light propagation in an atomic medium with steep and sign-reversible dispersion,” Phys. Rev. A **67**, 011801 (2003).

27- C. Andreeva, S. Cartaleva, and Y. Dancheva, “Coherent spectroscopy of degenerate two-level systems in Cs,” Phys. Rev. A **66**, 012502 (2002).

28- C. Goren, A. D. Wilson-Gordon, M. Rosenbluh, and H. Friedmann, “Atomic four-level *N* systems,” Phys. Rev. A **69**, 053818 (2004).

29- A. V. Taichenachev, A. M. Tumaikin, and V. I. Yudin, “On the spontaneous-coherence-transfer-induced sign change of a sub-natural-width nonlinear resonance,” JETP Lett. **69**, 819 (1999).

30- T. Zigdon, A. D. Wilson-Gordon, and H. Friedmann, “Pump-probe spectroscopy in degenerate two-level atoms with arbitrarily strong fields,” Phys. Rev. A **77**, 033836 (2008).

31- K. Dahl, L. S. Molella, R.H. Rinkleff, and K. Danzmann, “Switching from “absorption within transparency” to “transparency within transparency” in an electromagnetically induced absorption dominated transition,” Opt. Lett. **33**, 983 (2008).

32- H-u. Rehman, M. Adnan, H. R. Noh, and J. T. Kim, “Spectral features of electromagnetically induced absorption in ^{85}Rb atoms,” J. Phys. B **48**, 115502 (2015).

33- K. K. B. MacAdam, A. Steinbach, and C. Wieman, “A narrow-band tunable diode laser system with grating feedback, and a saturation absorption spectrometer for Cs and Rb,” Am. J. Phys **60**, 1098 (1992).

34- M. D. Levenson and S. S. Kano, “Introduction to Nonlinear Laser Spectroscopy,” Academic Press, Boston, (1988).

35- A. Banerjee, and V. Natarajan, “Saturated-absorption spectroscopy:

eliminating crossover resonance by use of co-propagating beams," Opt. Lett. 28, **1912** (2003).

36- C. E. Wieman, L. Hollberg, "Using diode laser for atomic physics," Rev. Sci. Inst. **62**, 1 (1990).

37- L. Ricci, M. Weidemuller, T. Esslinger, A. Hemmerich, C. Zimmermann, V. Vuletic, W. Kong, and T. W. Hansch, "A compact grating-stabilized diode laser system for atomic physics," Opt. Comm.**117**, 541 (1995).

38- K. B. MacAdam, A. Steinbach, and C. Weiman, "A narrow-band tunable diode laser system with grating feedback, and a saturated absorption spectrometer for Cs and Rb," Am. J. Phys. **60**, 1098 (1992).

39- C. Weiman, and L. Hollberg, "Using diode laser for atomic physics," Rev. Sci. Instrum. **62**, 1 (1991).

40- "Saturation Absorption Spectroscopy" University of Florida-Department of Physics (PHY 4803L – Advanced Physics Laboratory)

41- H.-R. Noh, "*Optical pumping and spectroscopic line shapes*", (Chonnam National University) 2009.

42- H.-R. Noh, "*Magneto-optical trapping of rubidium atoms: isotopes separation and cold collisions*," (Seoul National University) 1996.

43- F. L. Kien, and K. Hakuta, "*Density operator and applications in nonlinear optics,*" (University of Electro-Communications, Chofu, Tokyo) 2004.

44- Georgia Institute of Technology lab manual, "*Measuring the hyperfine levels of rubidium using saturation absorption spectroscopy*,"
http://advancedlab.physics.gatech.edu/labs/SaturationSpectroscopy/S

atSpecManual.pdf

45- H. Ur Rehman, *"Study on spectral features of electromagnetically induced absorption in degenerate two-level system of ^{85}Rb atoms"* (Chosun University) 2015.

46- . H. Ur Rehman, M. M. Qureshi, H.-R. Noh, and J. T. Kim, "Ultra-narrow electromagnetically induced absorption due to transfer of coherence and population for the $F_g = 3 \rightarrow F_e = 4$ transition in ^{85}Rb atoms", submitted to J. Phys. B (2015).

Appendix A

This appendix provides a brief review of the fine and hyperfine structures of D_2 line of the ^{85}Rb and ^{87}Rb atoms.

Rubidium is in IA alkali metal group in the periodic table with ground state electronic configuration of $1s^2$, $2s^2$, $2p^6$, $3s^2$, $3p^6$, $4s^2$, $3d^{10}$, $4p^6$, $5s^1$. The next higher energy configuration has the 5s valence electron promoted to a 5p orbital with no orbital change of the remaining 36 electrons. This means that the $L\left(\text{sum of } l_i\right)$ and $S\left(\text{sum of } s_i\right)$ for all 36 electrons in the filled orbitals is zero and only a valence electron contributes their values for the ground state and excited state.

Fine structure: In rubidium atom only one electron is a valence electron so that orbital angular momentum and spin due to the valence electron are

$$L = 0$$
$$S = 1/2$$

Thus the only possible value for total angular momentum $\boldsymbol{J} = \boldsymbol{L} + \boldsymbol{S}$ is

$$J = 1/2 \qquad \text{(A1)}$$

Therefore the ground state term symbol $^{(2S+1)}L_J$ can be described as $^2S_{1/2}$.

But for the case of excited state, a valence electron is in *5p* orbital then,

$$L = 1$$
$$S = 1/2$$

Then two different values of $\boldsymbol{J} = \boldsymbol{L} + \boldsymbol{S}$ from the following formula are possible.

$$J = |L - S| \text{ to } |L + S|$$

$$J = \left|1 - \tfrac{1}{2}\right| \text{ and } J = \left|1 + \tfrac{1}{2}\right|$$

$$J = \left|\tfrac{1}{2}\right| \text{ and } J = \left|\tfrac{3}{2}\right| \quad \text{(A2)}$$

Thus term symbol of the excited state $^{(2S+1)}L_J$ has two different forms with $^2P_{1/2}$ and $^2P_{3/2}$. Such fine structure of the ground and first excited states can be picturized in Fig. A1.

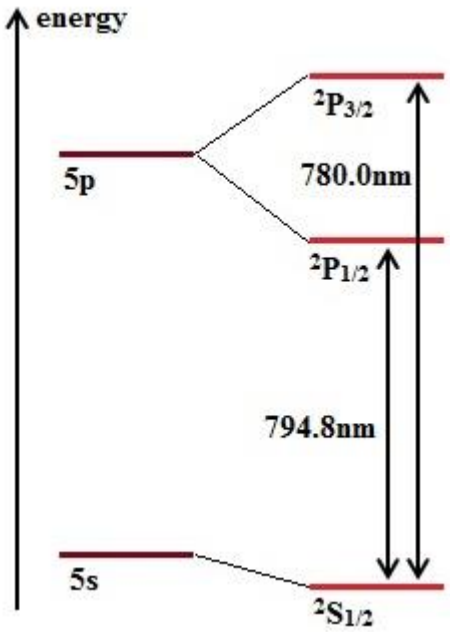

Fig. A1: Fine structure of the ground and first excited states for both ^{85}Rb and ^{87}Rb atoms.

Hyperfine structures of rubidium

Although ^{85}Rb and ^{87}Rb atoms have same fine structures, hyperfine structures have different structures due to different nuclear spins of those atoms. The range of F values is

$$|I-J| < F < |I+J|.$$

(a) ^{85}Rb atom

Nuclear spin I of ^{85}Rb is $I = 5/2$. From equation (A1) for ground state,

$$5^2S_{1/2} \rightarrow J = 1/2$$

Then, ground state hyperfine quantum number (F) is

$$F = \left|1/2 - 5/2\right| \text{ to } \left|1/2 + 5/2\right|$$

$$F = 2 \text{ to } F = 3.$$

For excited state equation (A2)

$$5^2P_{1/2} \rightarrow J = 3/2$$

Then, excited state hyperfine *(F')*

$$F' = \left|1/2 - 5/2\right| \text{ to } \left|1/2 + 5/2\right|$$

$$F' = 2 \text{ to } F' = 3$$

Similarly, for excited state equation (A2)

$$5^2P_{3/2} \rightarrow J = 3/2$$

Then, excited state hyperfine (*F'*)

$$F' = \left|3/2 - 5/2\right| \text{ to } \left|3/2 + 5/2\right|$$

$$F' = 1 \text{ to } F' = 3$$

Such hyperfine structure of the ground and first excited states can be picturized in Fig. A2.

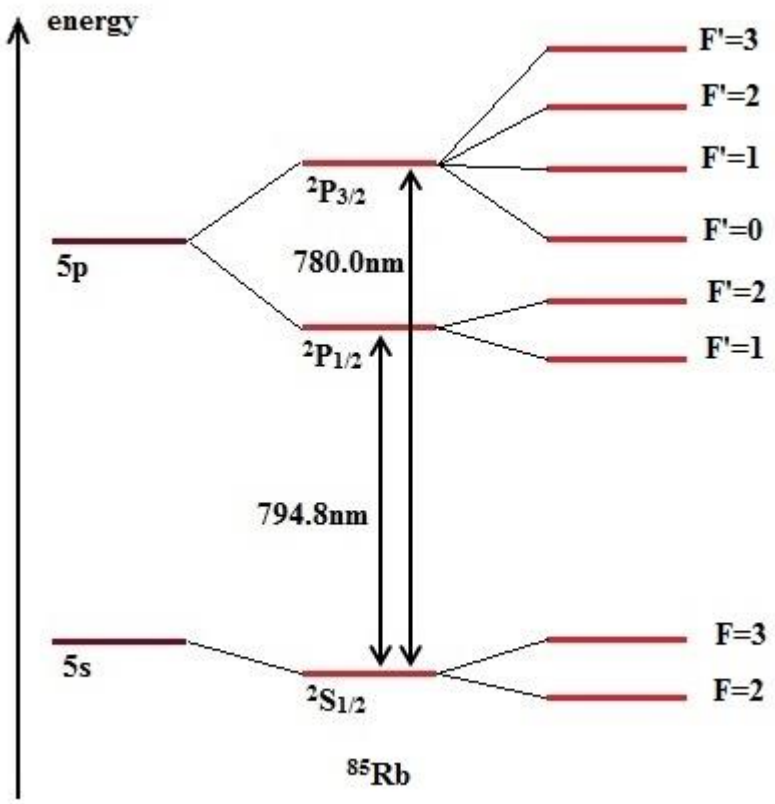

Fig. A2. Hyperfine structure of the ground and first excited states of the ^{85}Rb atom.

(b) ^{87}Rb Calculation

Similarly we can describe hyperfine structure of ^{85}Rb atom. Hyperfine quantum number F is

$$|I - J| < F < |I + J|$$

Because nuclear spin I for ^{87}Rb is $I = 3/2$. From equation (A1) for ground

state,

$$5^2S_{1/2} \rightarrow J = 1/2$$

Then, ground state hyperfine (F) has

$$F = \left|1/2 - 3/2\right| \text{ to } \left|1/2 + 3/2\right|$$

$$F = 1 \text{ to } F = 2 .$$

For excited state equation (A2)

$$5^2P_{1/2} \rightarrow J = 1/2$$

Then, excited state hyperfine *(F')*

$$F' = \left|1/2 - 3/2\right| \text{ to } \left|1/2 + 3/2\right|$$

$$F' = 1 \text{ to } F' = 2$$

Similarly, for excited state equation (A2)

$$5^2P_{3/2} \rightarrow J = 3/2$$

Then, excited state hyperfine *(F')*

$$F' = \left|3/2 - 3/2\right| \text{ to } \left|3/2 + 3/2\right|$$

$$F' = 0 \text{ to } F' = 3$$

Such hyperfine structure of the ground and first excited states can be picturized in Fig. A2.

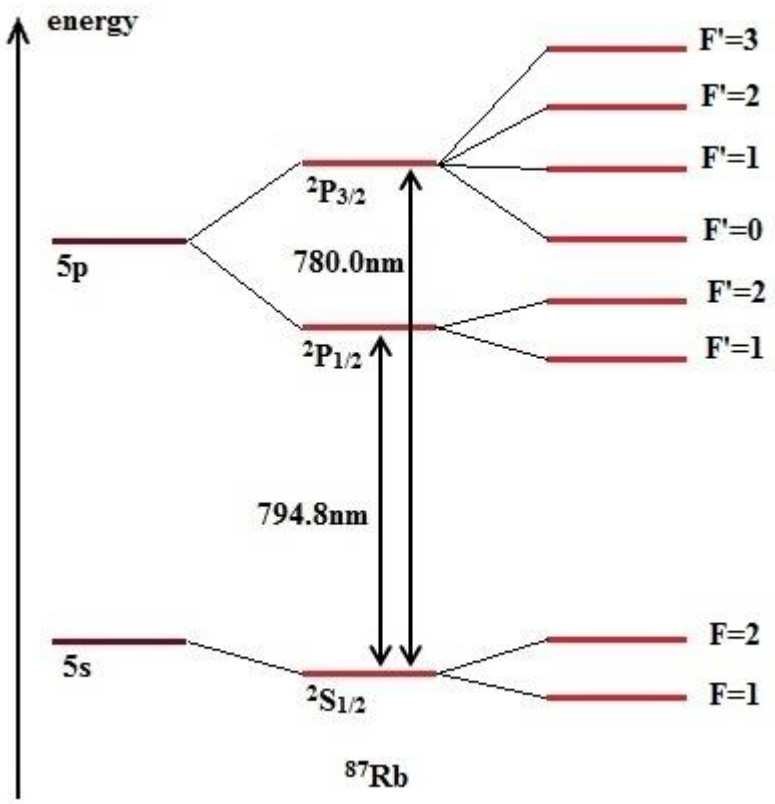

Fig. A3: Energy diagram of hyperfine structure of the ^{87}Rb atom.

Appendix B

Equation (3.27) implies that

$$\dot{\sigma}_{ij} = e^{-iK_{ij}t} Q_{ij} - iK_{ij}\sigma_{ij}$$

In this appendix we solve the first equation in which $i=j=e$, then,

$$\dot{\sigma}_{ee} = e^{-iK_{ee}t} Q_{ee} - iK_{ee}\sigma_{ee} \tag{B1}$$

From equation (3.28),

$$K_{ee} = 0$$

Therefore,

$$\dot{\sigma}_{ee} = Q_{ee} \tag{B2}$$

The formula for Q_{ee} is obtained from equation (3.30),

$$Q_{ee} = -\frac{i}{\hbar}\left[H_A + H_1 + H_2, \rho\right] + \left(\dot{\rho}\right)_{sp}$$

$$Q_{ee} = -\frac{i}{\hbar}\left\{\left(H_A + H_1 + H_2\right)\rho - \rho\left(H_A + H_1 + H_2\right)\right\} + \left(\dot{\rho}\right)_{sp}$$

Substituting the value of $\left(\dot{\rho}\right)_{sp}$ from table 3.1, we have

$$Q_{ee} = -\frac{i}{\hbar}\left\{\left(H_A + H_1 + H_2\right)\rho - \rho\left(H_A + H_1 + H_2\right)\right\} - \gamma\rho_{ee}$$

$$\because \rho_{ee} = \sigma_{ee} e^{iK_{ee}t} = \sigma_{ee}\left(1\right) = \sigma_{ee}$$

$$Q_{ee} = -\frac{i}{\hbar}\left\{\left(H_A + H_1 + H_2\right)\rho - \rho\left(H_A + H_1 + H_2\right)\right\} - \gamma\sigma_{ee} \tag{B3}$$

In the case of ladder configuration, H_1 is equal to zero because we know that

there is no connection between $|e\rangle$ and $|g\rangle$ from Fig. (3.3).

Thus equation (B3) can be written as,

$$Q_{ee} = -\frac{i}{\hbar}\left\{\left(H_A + H_2\right)\rho - \rho\left(H_A + H_2\right)\right\} - \gamma\sigma_{ee}$$

Substituting the values of H_A and H_2 from equation (3.23), we have the followings;

$$Q_{ee} = -\frac{i}{\hbar}\left\{\begin{aligned}&\hbar\left(\omega_{10}+\omega_{20}\right)|e\rangle\langle e|e\rangle\langle e| + \hbar\omega_{10}|r\rangle\langle e|e\rangle\langle e| \\ &+\frac{1}{2}\hbar\Omega_2 e^{-i\omega_2 t}|e\rangle\langle r|e\rangle\langle e| + \frac{1}{2}\hbar\Omega_2 e^{i\omega_2 t}|r\rangle\langle e|e\rangle\langle e|\end{aligned}\right\}$$
$$-\frac{i}{\hbar}\left\{\begin{aligned}&\hbar\left(\omega_{10}+\omega_{20}\right)|e\rangle\langle e|e\rangle\langle e| + \hbar\omega_{10}|e\rangle\langle e|r\rangle\langle r| \\ &+\frac{1}{2}\hbar\Omega_2 e^{-i\omega_2 t}|e\rangle\langle e|e\rangle\langle r| + \frac{1}{2}\hbar\Omega_2 e^{i\omega_2 t}|e\rangle\langle e|r\rangle\langle e|\end{aligned}\right\} - \gamma\sigma_{ee}$$

$$\therefore \langle e|e\rangle = 1$$
$$\langle r|e\rangle = \langle e|r\rangle = 0$$

$$Q_{ee} = -\frac{i}{\hbar}\left\{\hbar\left(\omega_{10}+\omega_{20}\right)\rho_{ee} + 0 + 0 + \frac{1}{2}\hbar\Omega_2 e^{i\omega_2 t}\rho_{er}\right\}$$
$$-\frac{i}{\hbar}\left\{\hbar\left(\omega_{10}+\omega_{20}\right)\rho_{ee} + 0 + 0 + \frac{1}{2}\hbar\Omega_2 e^{-i\omega_2 t}\rho_{re}\right\} - \gamma\sigma_{ee}$$

$$\therefore e^{i\omega_2 t}\rho_{er} = \sigma_{er}$$
$$e^{-i\omega_2 t}\rho_{re} = \sigma_{re}$$

$$Q_{ee} = -\gamma\sigma_{ee} + \frac{i}{2}\left(\sigma_{er} - \sigma_{re}\right)$$

Substituting value in equation (B2), finally we have the following relation.

$$\dot{\sigma}_{ee} = -\gamma\sigma_{ee} + \frac{i}{2}\left(\sigma_{er} - \sigma_{re}\right)$$

Appendix C

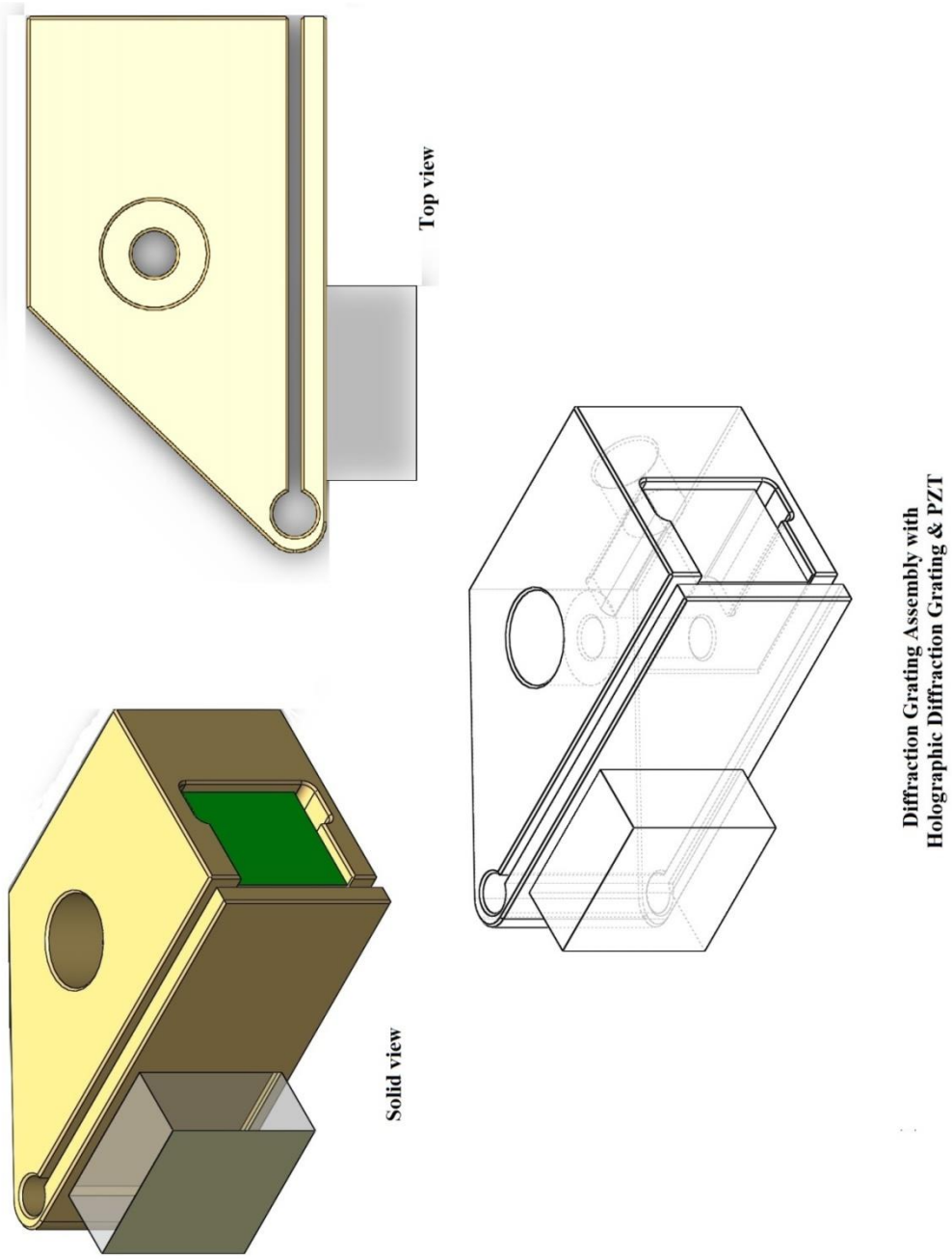

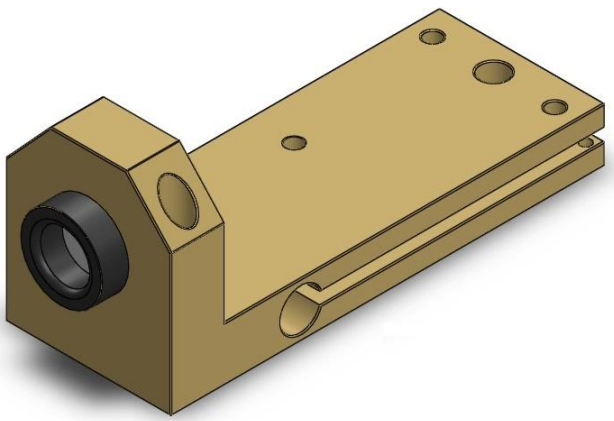

Solid View

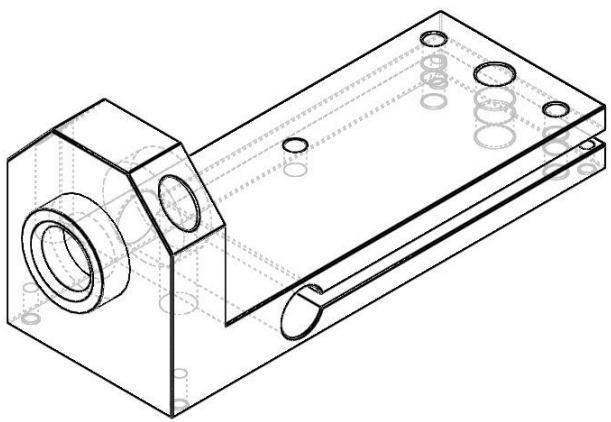

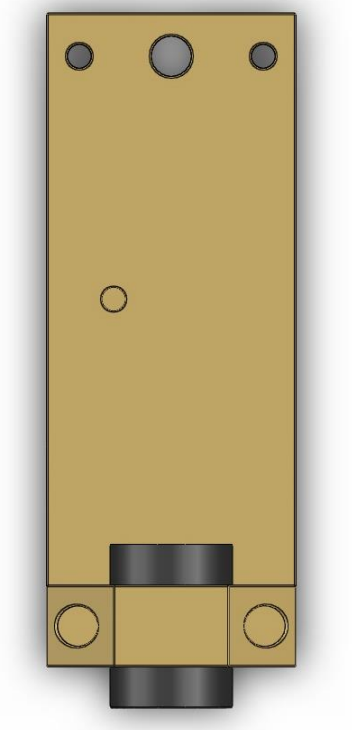

Top View

Diode laser holder with base plate

External Cavity Diode Laser (ECDL)

Acknowledgement

I would like to thank my advisor Professor Jin-Tae Kim for his guidance and support over the course of this research. He has taught me not only about spectroscopy, but also about how to be a good researcher, experimentalist, and scientist. I have worked with my advisor in this project, his knowledge, theoretical and experimental expertise, and skills are always beyond the amazement to me. I am not sure that I could ever be better than him. I would also like to express gratitude to him for his encouragement, and financial support as a part of this research.

I would also like to acknowledge Professor Heung-Ryoul Noh from Chonnam University, for his guidance and sharing of his precious knowledge. I am very lucky to have a chance to work with him, who is very genius but also very kind.

It has been a great opportunity for me to do my research in Laser Application Laboratory, Department of Photonic Engineering, Chosun University. All faculty members of department of Photonic Engineering have helped me in some ways on this research. I would like to thank Professor Hyun-Su Kim, Professor Jong-Rak Park, Professor Tae-Jung Ahn, Professor Min-Ki Gwon, and Professor Ki-Nam Joo for their enormous supports. I would also like to thank Dr. Pavlo V. Yezhov for his encouragement and useful discussion about Matlab and holography.

My special thanks to Dr. Hafeez-ur-Rehman for his assistance and useful discussion for keeping the laser and related equipment in best conditions and also for his valuable discussion.

My mother Sharf Qabila, who encouraged me to come over to Korea for higher studies, deserves to get more applause than anyone else. Without her,

I wouldn't be here today. It's because of her continuous prays, and support that every hurdle in my way to complete this research gets vanish. It is her dream for me to become a successful person in life and I confidently say that today her dream comes true. I dedicated this thesis to my mother. I also want to pay tribute to my father (late) who was my first teacher of Algebra and Mathematics. Lastly, I owe priceless appreciation to my elder brothers and sisters who encouraging me with their best wishes.

Finally, I give thanks to my friends in Chosun University and GIST. All of them were always there cheering me up and stood by me through the good times and bad in Korea.